BubR1 and Mad2 regulate adult midgut remodeling in *Drosophila* diapause

Yuya Adachi[1], Hiroki Nagai[1,2†], Tenki Nakasugi[1†], Miyu Nagao[1†], Hiroko Nakatani[1], Takako Fujichika[3], Aya Takahashi[3], Masayuki Miura[1], and Yu-ichiro Nakajima[1*]

1. Laboratory of Genetics, Graduate School of Pharmaceutical Sciences, The University of Tokyo, Japan
2. Institute of Science and Technology Austria, Austria
3. Department of Biological Sciences, Tokyo Metropolitan University, Japan

[†]These authors contributed equally.

*Author for correspondence e-mail: nakaji97@g.ecc.u-tokyo.ac.jp

Tel: +81-3-5841-4863

Text: 28,227 characters

Figures: 5

Supporting information: Supplemental figures S1-S4, Supplemental table S1-S5

Summary

Diapause is a survival strategy in which growth and aging are temporarily suspended, enabling animals to withstand unfavorable environments. Various insects, including the fruit fly *Drosophila*, enter reproductive diapause, or dormancy, in response to colder temperatures and/or shorter day lengths. During reproductive diapause, ovarian development halts, and non-reproductive organs also undergo remodeling at both morphological and metabolic levels: however, the mechanisms underlying this remodeling and its physiological impact remain largely unclear. Here, we show that the *Drosophila* adult midgut undergoes extensive remodeling in diapause, marked by a sustained suspension of growth due to the cell cycle arrest of intestinal stem cells (ISCs) that revert to normal upon returning to recovery conditions. During dormancy, BubR1 and Mad2, key regulators of mitosis, are highly expressed and localized in the cytoplasm of ISCs rather than at the kinetochore, and both BubR1 and Mad2 are essential for diapause-specific midgut remodeling. Furthermore, disruption of midgut growth arrest during diapause reduces the resistance to starvation in adult flies. Together, our findings identify a novel role for BubR1 and Mad2 in ISCs–promoting proper midgut remodeling during dormancy–and highlight the importance of this process for survival under adverse environments.

Introduction

Wild animals have developed a wide array of survival strategies to cope with harsh environmental conditions such as temperature fluctuations, drought, and food shortages. Among these strategies, dormancy programs (e.g. hibernation, torpor, and diapause) are critical adaptations that involve a reduction in metabolic rate and body temperature, which conserves energy, extends lifespan, and increases the probability of survival for the species (Easwaran & Montell, 2023; Staples, 2016; Wilsterman et al., 2021). By temporarily halting growth and delaying organ development under stressful conditions such as starvation and low temperatures, dormancy helps reduce the energy expenditure required for growth and reproduction, and this synchronization of physiological processes with environmental conditions enhances the organism's ability to survive (Denlinger, 2022; Schiesari & O'Connor, 2013). Understanding the underlying mechanisms of dormancy may thus provide valuable insights into the regulation of stress resistance, aging, and reproduction.

Dormancy programs typically comprise three distinct phases: a preparatory phase in which environmental cues initiate dormancy; a dormancy phase characterized by reduced metabolism and activity; and a recovery phase wherein normal growth and activity resume (Gray et al., 1991; Harsimran Kaur Gill et al., 2017). To enter and exit dormancy at the appropriate time, animals must be able to successfully detect environmental conditions and coordinate internal physiological processes. As such, dormancy regulation generally requires central control mechanisms involving the brain and endocrine systems (Helfrich-Förster, 2024; Karp, 2021). While hormonal and neural regulation play pivotal roles in directing these processes, peripheral organs and tissues must also undergo significant remodeling during dormancy and subsequent reversion during recovery. For instance, during hibernation in certain mammals (e.g. thirteen-lined ground squirrels, Syrian hamsters) and diapause in insects, structural changes are observed in respiratory and digestive organs as well as in muscles and adipose tissues (Kim et al., 2006; Kim & Denlinger, 2009; Kurtz et al., 2021). Despite these substantial transformations and their vital importance, the mechanisms by which cellular compositions within individual organs and

tissues are precisely coordinated to adjust dormancy programs remain largely unknown.

Animal species enter dormancy at different life stages, and in adult insects, dormancy is often referred to as reproductive diapause, a state that suppresses reproductive organ development and is associated with reduced locomotor activity, lower metabolism, increased stress resistance, and extended lifespan(Denlinger, 2022; Tatar & Yin, 2001). In species like *Drosophila*, reproductive diapause is triggered by low temperatures and/or short-day conditions (Hara & Yamamoto, 2022; Lirakis et al., 2018; Ojima et al., 2018; Saunders et al., 1989). As with other diapausing insects, the reduction of juvenile hormone and insulin signaling are critical for maintaining reproductive diapause in *Drosophila* (Easwaran et al., 2022; Saunders et al., 1990; Schiesari et al., 2016). Recent studies have used *D. melanogaster* to explore the genetic basis of dormancy's complex biology and have resulted in the identification of circadian neurons that regulates the endocrine organs, the mechanism of germline maintenance, and sleeping behaviors (Easwaran et al., 2022; Kurogi et al., 2023; Meiselman et al., 2022; Meyerhof et al., 2024; Schiesari et al., 2016). Interestingly, similar to dormancy programs in other animals, somatic non-reproductive organs such as the midgut undergo structural changes during reproductive diapause in *Drosophila* (Kubrak et al., 2014); however, the mechanism by which the dormant state regulates organ remodeling and its physiological impacts remain unclear.

The *Drosophila* adult midgut, composed of a monolayered epithelium surrounded by visceral muscle, is home to resident intestinal stem cells (ISCs) that self-renew and give rise to committed progenitors, enteroblasts (EBs) and enteroendocrine progenitor cells (EEPs); these progenitors differentiate into absorptive enterocytes (ECs) and secretory enteroendocrine cells (EEs), respectively (Hung et al., 2020; Miguel-Aliaga et al., 2018; see also Fig. 2A, 2B). To achieve adaptive responses to environmental changes at the organ level, the ISC lineage exhibits characteristic behaviors that enable proper tissue homeostasis and plasticity (Nagai et al., 2022; O'Brien et al., 2011). Furthermore, the midgut plays a central role in regulating organism-level physiology, influencing appetite, fecundity, immunity, and lifespan (Malita et al., 2022; White et al., 2021; Yoshinari et al., 2024; Zhou et al., 2020). With its relatively simple

117 structure and conserved cell lineages, the *Drosophila* adult midgut serves an
118 ideal system for dissecting the mechanisms of organ remodeling associated with
119 environmental challenges like dormancy.

120 Here, we investigate the mechanistic underpinnings of organ remodeling
121 during diapause, using the *Drosophila* adult midgut as a model. Our results show
122 that intestinal growth halts during dormancy and resumes during recovery,
123 accompanied by changes in structural and metabolic gene expression. We
124 identify mitotic regulators BubR1 and Mad2, which are highly expressed in the
125 cytoplasm of ISCs, as key players in midgut remodeling during diapause, and
126 show that disruption of these genes leads to abnormal gut size and a reduced
127 capacity for starvation resistance. These findings suggest novel roles of BubR1
128 and Mad2 in controlling ISCs dynamics and contributing to midgut remodeling in
129 *Drosophila* diapause.
130
131

132 Results

133 The adult midgut of *D. melanogaster* undergoes remodeling in response to 134 diapause and recovery

135 In adult females of *D. melanogaster*, reproductive diapause can be induced by
136 exposing newly eclosed flies to cold temperatures (below 12°C), halting ovarian
137 development at an early stage (Anduaga et al., 2018). Following previous studies
138 (Easwaran et al., 2022; Kubrak et al., 2014; Saunders et al., 1989), we kept newly
139 eclosed flies at short-day photoperiods (10L:14D) and 10°C while non-diapause
140 control flies were kept at 12L:12D and 18°C (Fig. 1A). Under this suboptimal
141 condition, females were confirmed to have entered reproductive dormancy as no
142 yolk accumulation was observed in the ovaries (Fig. S1A). To assess changes in
143 midgut size during diapause, we measured the length and area of the midgut in
144 the wild-type fly (Canton-S) under diapause and non-diapause conditions for 1 to
145 5 weeks. Consistent with previous findings (Kubrak et al., 2014), we confirmed
146 that midgut length remained shorter during diapause compared to non-diapause
147 conditions (Fig. 1B, 1C), while becoming similar to that immediately after eclosion
148 (Fig. 1C). After one week of recovery from diapause, the midgut significantly
149 increased in size (Fig. 1B, 1D, Fig. S1B, S1C) and fully recovered by day 4 (Fig.

150 S1D). Of note, after 5 weeks of diapause, no significant midgut growth occurred
151 upon recovery (Fig. 1D), suggesting the existence of a time limit on the midgut's
152 ability to regrow. These findings together indicate that the midgut halts growth
153 during diapause but remains capable of rapid regrowth upon recovery.

154 The *Drosophila* adult midgut consists of anterior (R1-R2), middle (R3),
155 and posterior regions (R4-R5) (Buchon et al., 2013; Marianes & Spradling, 2013).
156 Since these regions respond differently to environmental changes due to the
157 divergent nature of ISCs and their progenies (Li & Jasper, 2016; Mattila et al.,
158 2024; Nagai et al., 2023; O'Brien et al., 2011), we analyzed midgut size changes
159 in the anterior and posterior regions under the 3-week diapause condition where
160 the difference between diapause and non-diapause midgut size is greatest (Fig.
161 1C). We found that the posterior midgut differed more significantly across
162 conditions (Fig. 1E) than the anterior midgut. Similar region-specific gut resizing
163 during diapause and recovery was also observed in the w^{1118} strain (Fig. 1F),
164 suggesting that the posterior region is preferentially affected during dormancy. It
165 has been reported that reproductive development is also suppressed in
166 *Drosophila* adult males under the same conditions females enter diapause
167 (Kubrak et al., 2016). To assess diapause's effect on the midgut across sexes,
168 we measured midgut size in males under diapause and non-diapause conditions
169 but ultimately found no significant differences between the two (Fig. S1G). These
170 observations suggest that midgut remodeling in diapause is a sexually dimorphic
171 trait, appearing only in females.

172 To determine whether the observed midgut remodeling is specific to
173 diapause or is rather a general response to cold-induced stress, we exposed
174 female flies to the cold temperature conditions outlined above after the midgut
175 had matured and ensuring no diapause was induced (Ojima et al., 2018).
176 Comparing the midgut size after 3 weeks under cold and diapause conditions,
177 we found that midgut size was larger under cold conditions (Fig. S1E, S1F).
178 Furthermore, midgut growth was not observed when flies were transferred from
179 the cold condition to recovery, contrary to the transition observed during diapause
180 recovery (Fig. S1F). Altogether, these results suggest that midgut remodeling is
181 a diapause-specific response in adult females in which midgut growth is halted in

182 a regrowth-ready state. We term this midgut remodeling during diapause:
183 “dormancy-dependent midgut remodeling” (DDMR).
184
185 **Midgut remodeling as a common response in *Drosophila* species**
186 While the model organism *D. melanogaster* has recently been used as a genetic
187 model to study numerous aspects of diapause (Easwaran et al., 2022; Easwaran
188 & Montell, 2024; Meiselman et al., 2022; Ojima et al., 2018), it is still unclear
189 whether this species naturally enters diapause in the wild (Lirakis et al., 2018).
190 However, it has been established that some species of the genus *Drosophila*
191 undergo a programmed state of diapause in response to environmental changes
192 like short-day lengths that enables them to survive through the winter (Kimura,
193 1990; Lakovaara et al., 1972).
194 To explore whether DDMR is a general organ-level response during
195 reproductive dormancy, we examined two other *Drosophila* species: *D. bifasciata*
196 and *D. triauraria* (Fig. 1G), which inhabit northern regions and have been shown
197 to halt ovarian development in short-day seasons (Watabe, 1979; Yamada &
198 Yamamoto, 2011). We confirmed that these species exhibit reproductive
199 diapause under short-day conditions (SD, 10L: 14D), while such diapause was
200 not induced in long-day conditions (LD, 16L: 8D) at the same moderate
201 temperature (15°C) (Fig. 1H, S1H). In SD, midgut size was significantly smaller
202 compared to LD, and midgut regrowth was observed during recovery (Fig. 1I-1K).
203 Notably, this midgut growth arrest was not observed in non-diapause strains of
204 *D. triauraria* that originate from southern regions (Yamada & Yamamoto, 2011)
205 (Fig. S1I, S1J). These results support the notion that DDMR in *D. melanogaster*
206 represents a general organ-level response triggered during diapause in the
207 genus *Drosophila*.
208
209 **ISCs maintain cell cycle arrest and inhibition of mitosis during diapause**
210 In the adult midgut epithelium of *Drosophila*, ISCs serve as resident stem cells,
211 maintaining the self-renewing population and producing progenitors (EBs and
212 EEPs) that further differentiate into absorptive ECs and secretory EEs,
213 respectively (Fig. 2A, 2B; Hung et al., 2020; Miguel-Aliaga et al., 2018).
214 Previous studies have shown that alterations in cell number via ISC expansion

215 and reduction contribute to the substantial midgut size changes that correspond
216 with environmental fluctuations (Christensen et al., 2024; Nagai et al., 2022;
217 Stojanović et al., 2022). For example, after mating, juvenile hormones stimulate
218 ISC proliferation, leading to an increase in midgut size (Reiff et al., 2015).
219 Similarly, upon refeeding following starvation, ISC symmetric division is
220 promoted in the posterior midgut (O'Brien et al., 2011), resulting in ISC
221 expansion and a subsequent increase in total cell number as well as midgut
222 size.

223 To investigate whether changes in cell number contribute to midgut
224 remodeling in diapause, we first quantified the midgut cell abundance following
225 3 weeks of diapause. We observed a significant reduction in total cell number
226 during diapause compared to non-diapause conditions (Fig. 2C). We then
227 examined the number of ISC/EB lineage using the protein trap line *esg-GFP.*
228 The number of *esg*+ cells, along with their relative proportion, was markedly
229 lower during diapause, especially in the posterior midgut (Fig. 2D, 2E, Fig.
230 S2A). Consistent with this observation, the ISC marker *Delta* (*Dl*) and the EB
231 marker *Su(H)* exhibited reduced expression in the diapausing midgut (Fig. S2B-
232 S2F). Moreover, *esg*+ cell number dramatically increased during recovery from
233 diapause, coinciding with midgut regrowth (Fig. 2E). These findings suggest the
234 possibility that ISCs remain in a non-proliferative state during diapause and
235 resume proliferation upon recovery.

236 To test this possibility, we investigated ISC mitotic activity using the
237 anti-phospho-Histone H3 (PH3) immunostaining, a marker for mitotic cells.
238 Unexpectedly, we found that the number of ISCs in the M phase significantly
239 increased in both the anterior and posterior midgut during diapause (Fig. 2F,
240 2G). Despite the reduced number of ISCs (Fig. 2E, S2B, S2C), the increase in
241 mitotic cells suggests that ISCs may arrest the cell cycle in the M phase or,
242 alternatively, experience prolonged M phase during diapause.

243 In order to directly test ISC proliferative capacity, we conducted clonal
244 expansion assays using the mosaic analysis with a repressible cell marker
245 (MARCM) system (Fig. 2H) and found that clonal size was significantly reduced
246 during diapause, with fewer ISCs present in the clones (Fig. 2I, 2J). This mitotic

247 arrest was not observed during recovery from diapause, with the number of
248 mitotic cells returning to non-diapause levels (Fig. S2G).
249 To further examine the ISC lineage cell cycle state, we employed the
250 Fly-FUCCI system (Zielke et al., 2014) in combination with the *esg-QF* driver
251 during diapause. Using this system makes it possible to monitor the cell cycle at
252 cold temperatures, and we found that a significantly higher proportion of *esg*+
253 cells were in the G2/M phase during diapause compared to non-diapause
254 controls (Fig. 2K, 2L). Additionally, using the *CycB-GFP* line, we confirmed
255 increased *CycB* expression in ISCs during diapause (Fig. S2H), reinforcing the
256 idea that ISCs arrest in the G2/M phase. These results suggest that ISCs
257 undergo cell cycle arrest in the G2/M phase during dormancy.
258 Combined, our findings reveal that ISCs undergo drastic behavioral
259 changes during DDMR–that they effectively halt the cell cycle at a recoverable
260 state, reducing the number of cells produced post-eclosion and allowing for
261 proper size change during diapause.
262
263 **Molecular signatures of DDMR**
264 To explore the molecular signature of DDMR, we conducted a transcriptome
265 analysis of the midgut. Specifically, bulk RNA sequencing (RNA-seq) was
266 performed on samples of the entire adult midgut from two conditions: 3 weeks
267 diapause (3wD) and 3 weeks non-diapause control (3wC). We identified 3,391
268 genes that were differentially expressed during dormancy (Fig. 3A). Gene
269 Ontology (GO) enrichment analysis and Reactome pathway analyses revealed
270 that metabolic processes, including small molecule, lipid, and carboxylic acid
271 metabolism were significantly enriched in the 3wD midgut (Fig. S3A, S3B),
272 suggesting that large-scale metabolic remodeling occurs alongside structural
273 changes in the midgut during dormancy. Lipid metabolism-related genes such as
274 *bmm* and *pepck*, along with carbohydrate metabolism-related genes like *tobi*,
275 were differently expressed (Fig. S3C). Additionally, pathways related to
276 metabolism (e.g., Metabolism of Lipids), translation regulation (e.g., Translation),
277 and circadian gene degradation (e.g., Degradation of TIM) were among the top
278 processes identified (Fig. S3B). Notably, circadian genes *per* and *tim*, which are
279 upregulated in the entire body during diapause (Kučerová et al., 2016), also

280 showed significantly increased expression in the midgut during dormancy (Fig.
281 S3D). Furthermore, the expression of the antimicrobial peptide *Drs*, downstream
282 of the Toll pathway, dramatically increased during dormancy (Fig. S3E), reflecting
283 enhanced innate immunity, a hallmark of diapause at the organismal level
284 (Kubrak et al., 2014).

285 A detailed enrichment analysis was performed on the differentially
286 expressed genes, by categorizing the genes into two groups: those upregulated
287 during dormancy and those downregulated. In the upregulated gene group, GO
288 terms associated with cell adhesion and RNA processing (e.g., regulation of RNA
289 splicing) were identified as top-ranked categories (Fig. 3B). Genes associated
290 with RNA processing and RNA metabolism are also upregulated in the ovaries
291 during diapause, suggesting the existence of dormancy-specific translational
292 regulation conserved across organs (DiVito Evans et al., 2023). In the
293 downregulated gene group, by contrast, GO terms related to metabolic processes
294 (e.g., cellular lipid metabolic process) were prominently enriched (Fig 3C). During
295 diapause, extensive changes in the expression of genes involved in metabolic
296 pathways have been observed throughout the body (Kubrak et al., 2014;
297 Kučerová et al., 2016), and these findings suggest that gene expression changes
298 linked to DDMR globally follow a pattern similar to that observed in the entire
299 organism and other organs.

300 Next, to explore the molecular signature of DDMR recovery, RNA-seq
301 was performed using samples of the entire adult midgut from two conditions: 3
302 weeks diapause followed by recovery (3wD+R) and 3 weeks control followed by
303 recovery (3wC+R). We identified 526 genes with significant expression changes
304 between the 3wD+R and 3wC+R midguts (Fig. S3G). GO enrichment and
305 Reactome pathway analyses identified significant enrichment of genes
306 associated with muscle differentiation and smooth muscle contraction (Fig. S3H,
307 S3I). Given the extensive structural remodeling of muscles during insect
308 dormancy (Kim et al., 2006; Kim & Denlinger, 2009), these gene expression
309 changes related to muscle structure during recovery may contribute to the
310 resizing of the midgut. Consistent with this finding, *dilp3*, which codes the product
311 secreted by muscles during feeding and promote ISC proliferation (O'Brien et al.,
312 2011), was significantly upregulated in the 3wD+R midgut (Fig. S3J), suggesting

growth-promoting interactions between muscle and ISCs during recovery. In addition, neuropeptide genes such as *NPF, Dh31,* and *CCHa2* showed significant increases in expression (Fig. S3J), indicating that hormone secretion from EEs may change during recovery, potentially influencing gut growth and inter-organ communications. Overall, our findings suggest that the midgut undergoes large-scale structural and metabolic remodeling associated with extensive gene expression changes.

BubR1 expression increases in the cytoplasm of ISCs during diapause

Because ISC cell cycle are arrested during diapause (Fig. 2), we focused on differentially expressed genes categorized under the GO term “cell cycle checkpoint signaling” (Fig. 3D). G2/M phase checkpoint regulators such as *mre11*, *mei-41* showed significant changes while *CG15237* and *BubR1* were differentially expressed as M-phase checkpoint regulators. These gene expression changes align with ISC behaviors during dormancy such as prolonged mitotic phases and an increase in G2/M phase cells. Among these genes, *BubR1* is particularly noteworthy due to its established roles as a mitotic checkpoint regulator and mitosis timer (Karess et al., 2013) and its expression in ISCs (Shinoda et al., 2023). Importantly, *BubR1* expression increased nearly threefold during diapause (Fig. 3E), suggesting a major potential impact on ISC behaviors and midgut remodeling.

To investigate *BubR1* expression at the cellular level, we used fly lines, which allow for the detection of the endogenous expression pattern of *BubR1* (*EGFP::BubR1*^{WT} and *GFP-BubR1*) to visualize its expression in midgut cells. During reproductive dormancy, *BubR1* was strongly expressed in the cytoplasm of ISCs, primarily in R4 regions (Fig. 3F, 3G, S3F). This cytoplasmic localization during diapause contrasts with the localization of BubR1 associated with typical spindle checkpoint during mitosis, where it accumulates around kinetochores (Resende et al., 2018). Indeed, colchicine treatment, which induces mitotic arrest through the spindle assembly checkpoint (SAC), caused strong BubR1 localization around kinetochores in ISCs under non-diapause conditions (Fig. 3H, 3I). In contrast, during diapause, despite ISCs remaining arrested in mitosis, BubR1 remained cytoplasmic, with minimal signal around the

346 kinetochores (Fig. 3H, 3I). These findings suggest that the role of BubR1 during
347 DDMR is likely spindle checkpoint-independent and constitutes a unique
348 function in the midgut during the dormancy state.
349
350 **BubR1 expression in ISCs is essential for DDMR**
351 To explore the function of BubR1 in reproductive dormancy, we examined its
352 effects on midgut remodeling using two *BubR1* mutant alleles *BubR1*^{k06109} and
353 *BubR1*^{k03113}. qPCR analysis revealed that midgut *BubR1* expression in
354 diapause-induced flies was significantly reduced in both heterozygous mutants,
355 with *BubR1*^{k03113} showing 48% and *BubR1*^{k06109} showing 57% expression
356 compared to controls (Fig. 4A). We then measured midgut size during diapause
357 in these mutants and found a significant increase in midgut size compared to
358 control flies (Fig. 4B, 4C). This midgut enlargement was accompanied by an
359 increase in the total cell number, the number of mitotic ISCs, as well as the
360 number of *esg*+ cells (Fig. 4D-4F). Importantly, when BubR1 function was
361 rescued in the *BubR1* trans-heterozygous mutant (*BubR1*^{k06109}/*BubR1*^{k03113})
362 with an *EGFP::BubR1*^{WT} transgene (Shinoda et al., 2023), the total cell number
363 in the posterior region and mitotic cell number in the midgut returned to levels
364 comparable to controls (Fig. 4C-4E). These results strongly suggest that BubR1
365 is required for proper midgut remodeling during diapause. Notably, no ovarian
366 development was observed in any of the dormant mutants, confirming the
367 successful induction of ovarian dormancy despite impaired midgut remodeling
368 (data not shown). Furthermore, no significant differences in midgut size were
369 detected between these mutant backgrounds under non-dormant conditions
370 (Fig. S4A), consistent with the result that the number of mitotic cells did not
371 increase—or even decreased— in *BubR1* mutants (Fig. S4B). Collectively,
372 these results highlight a critical role for BubR1 in DDMR.
373 The results obtained from the mutants could potentially reflect non-
374 autonomous effects of *BubR1* expressed in other tissues. We thus investigated
375 whether DDMR is influenced by BubR1 activity specifically in adult ISCs. To this
376 end, we employed somatic tissue-specific CRISPR-mediated depletion (Bier et
377 al., 2018; Meltzer et al., 2019), combined with the temperature-sensitive Gal80^{ts}
378 system (McGuire et al., 2003) to induce *BubR1* mutations in ISC lineages

379 before eclosion (Fig. 4G, S4C). When adult flies were shifted to dormancy
380 conditions, we observed a significant increase in midgut size in ISC/EB-specific
381 *BubR1* knockout flies (Fig. 4H). Furthermore, the number of total and mitotic
382 cells also increased in these somatic *BubR1* knockout lines (Fig. 4I, 4J).
383 Altogether, our results demonstrate that *BubR1* function in ISCs is essential for
384 midgut remodeling during reproductive diapause.
385 Intriguingly, in *D. bifasciata* and *D. triauraria,* which undergo a
386 programmed state of diapause in response to short-day length, *BubR1*
387 expression in the midgut is higher in diapausing flies under SD compared to
388 non-diapausing flies under LD (Fig. S4D, S4E). These results suggest a
389 potential role of BubR1 in DDMR for the genus *Drosophila* more broadly.
390
391 **The MCC component Mad2 is involved in DDMR**
392 During mitosis, BubR1 forms a complex with Mad2, Bub3, and Cdc20, which
393 constitute key components of the mitotic checkpoint complex (MCC) and
394 function cooperatively at the kinetochores (Musacchio, 2015). Our RNA-seq
395 analysis indicated that, in addition to *BubR1,* the expression levels of *mad2*
396 increased significantly during dormancy (Fig. 5A), though it was not identified as
397 a differentially expressed gene. Intriguingly, Mad2 can interact with BubR1 in
398 the cytoplasm of mammalian cells to regulate insulin signaling and metabolism
399 (Choi et al., 2016). This raises the possibility that Mad2 may play a critical role
400 in DDMR, independently of its role in the MCC.
401 To assess this potential role, we utilized the *GFP-Mad2* line to examine
402 *mad2* expression in the adult midgut and found it to be highly expressed in the
403 cytoplasm of ISCs during diapause (Fig. 5B, 5C), reminiscent of the cytosolic
404 localization of BubR1 (Fig. 3F, S3F). To further investigate the function of Mad2
405 during DDMR, we analyzed midgut size using two *mad2* mutant alleles: $mad2^{\Delta}$
406 and $mad2^{EY21687}$. Our analysis revealed that heterozygous *mad2* mutants had
407 significantly larger midguts during dormancy compared to controls (Fig. 5D, 5E).
408 We also found that the number of *esg*+ cells increased in the anterior and
409 posterior region of the midgut (Fig. 5F). These findings suggest that during
410 reproductive diapause, Mad2 is localized in the cytoplasm of ISCs similarly to
411 BubR1 and that the two proteins together regulate DDMR.

412

413 **DDMR enhances starvation resistance**

414 Halting organ growth during dormancy is thought to conserve energy, thereby
415 enhancing survival during periods of food scarcity, such as winter (Denlinger,
416 2022). In *Drosophila*, maintaining midgut size during reproductive diapause may
417 contribute to increased resistance to starvation. To test this hypothesis, we
418 compared starvation resistance between dormant *BubR1* mutants and controls.
419 Although dormancy generally enhances starvation resistance compared to non-
420 dormant states, *BubR1* ^{k03113} mutant flies exhibited significantly reduced
421 starvation resistance during dormancy (Fig. 5G). These results suggest that
422 BubR1/Mad2-mediated DDMR plays a critical role in enhancing starvation
423 resistance at the organismal level.

424

425

426 Discussion

427 In this study, we demonstrate that BubR1 and Mad2 play crucial roles in DDMR
428 in *Drosophila* by modulating ISC dynamics to achieve diapause-specific states.
429 While BubR1 and Mad2 are well-known as components of the MCC that localizes
430 to the kinetochore, we found that in the diapausing midgut, they are
431 predominantly localized in the cytoplasm of ISCs. Depletion of these proteins
432 causes misregulated midgut growth and leads to reduced starvation resistance
433 during diapause. Based on these findings, we propose that BubR1 and Mad2 act
434 as key regulators of the ISC cell cycle during diapause, enabling a reversible
435 state that facilitates recovery (Fig. 5H).

436 The *Drosophila* midgut undergoes extensive remodeling in response to
437 various internal and external stimuli that directly or indirectly influence ISC
438 activity (Christensen et al., 2024; Nagai et al., 2022; Stojanović et al., 2022).
439 During starvation, for instance, the midgut size decreases as ECs undergo
440 apoptosis, while upon refeeding, ISCs are stimulated by Dilp3 secreted from
441 visceral muscles, promoting symmetrical ISC division and restoring midgut size
442 (O'Brien et al., 2011). Similarly, during reproductive diapause—wherein food
443 intake is reduced by less than half (Kubrak et al., 2014)—mild starvation
444 responses may also contribute to midgut size reduction. Indeed, reproductive

445 arrest can be more readily induced by adding starvation conditions (Ojima et al.,
446 2018). Our RNA-seq data revealed increased *dilp3* expression and decreased
447 expression of the FoxO target gene *Thor* during recovery (Fig. S3J), suggesting
448 the possibility that Dilp3 secreted from muscles contributes to ISC activation as
449 it does in post-starvation refeeding. However, in contrast to the simple
450 starvation response, midgut cell death is minimal during diapause (Fig.S2I), and
451 ISC cell cycles are arrested at G2/M in a recoverable state (Fig. 2).
452 Furthermore, during reproductive arrest, germline stem cells in ovaries exhibit
453 behaviors markedly different from those observed during amino acid deficiency
454 responses (Easwaran et al., 2022). Collectively, these findings suggest that
455 organ-level responses during diapause are driven by a complex interplay of
456 environmental factors rather than by a simple starvation-induced mechanism.
457 Across species, developmental diapause typically involves a temporary
458 halt in the cell cycle that delays organ growth. For example, during pupal
459 diapause in the *Sarcophaga crassipalpis* brain and embryonic diapause in the
460 turquoise killifish, the cell cycle primarily arrests at the G0/G1 phase (Meller et
461 al., 2012; Tammariello & Denlinger, 1998). By contrast, most cells in silkworm
462 embryos are arrested in the G2 phase during diapause (Nakagaki et al., 1991).
463 In this study, we observed a significant increase in ISCs arrested at the G2/M
464 phase during DDMR. *Drosophila* oogenesis arrests during diapause due to
465 activation of the Chk2 DNA damage checkpoint (Easwaran et al., 2022), and
466 our findings suggest that similar mechanisms may govern growth arrest in the
467 midgut. Indeed, genes like *mre11* that are differentially expressed in the
468 diapausing midgut (Fig. 3D) are required for G2/M checkpoint activation (Song,
469 2005). Notably, ISCs exhibit active cell cycle arrest during diapause via
470 checkpoint mechanisms, rather than undergoing a passive delay induced by
471 low temperatures (Fig. S1E-S1F). This controlled cell cycle arrest in resident
472 stem cells may contribute to the pausing of organ growth in other diapausing or
473 hibernating animals and to facilitating rapid recovery once stem cell division
474 resumes.
475 BubR1 is a highly conserved eukaryotic protein that functions as a key
476 component of the SAC, forming the MCC with Mad2, Bub3, and Cdc20 to
477 prevent premature progression of cell division and ensure accurate

chromosomal segregation, and its disruption increases the risk of aneuploidy (Baker et al., 2013; Karess et al., 2013; Resende et al., 2018). Beyond these canonical functions, studies across cellular and organismal contexts have uncovered additional roles for BubR1. For example, in mouse embryonic fibroblasts, *BubR1* heterozygosity reduces *p53* and *p21* expression after DNA damage, impairing proper G2/M phase arrest (Fang et al., 2006). Additionally, BubR1, together with Mad2, recruits adaptor protein 2 to the insulin receptor (IR) to promote IR endocytosis and reduce insulin sensitivity (Choi et al., 2016; Park et al., 2023; Tang et al., 2020). Consistent with these findings, *BubR1* deficiency in mice leads to premature aging and reduced lifespan, highlighting its role in organism-wide responses (Baker et al., 2004). In *Drosophila*, BubR1 in the fat body negatively regulates *bmm* expression via IMD signaling during starvation, suppressing lipid breakdown and enhancing lifespan (Liu et al., 2024). These findings delineate a complex regulatory network involving BubR1 and associated proteins across different biological contexts. Although the regulation and interacting partners of BubR1 and Mad2 during diapause have yet to be identified, the observed changes in their expression in ISCs likely contribute to organism-level responses, including enhanced starvation resistance mediated by structural and metabolic changes in the midgut. Future investigations into these emerging additional roles of BubR1/Mad2 will enhance our understanding of organ remodeling in dormancy programs and provide new insights into the control of resident stem cells.

Acknowledgements

We thank R. Giet, B. Ohlstein, C. Sunkel, N. Shinoda, BDSC, Kyoto Stock Center, NIG-FLY, KYORIN-Fly, and Developmental Studies Hybridoma Bank (DSHB) for fly stocks and reagents; Y. Hara and S. Kondo for discussion.

Funding

This work was supported by JSPS/MEXT KAKENHI (grant numbers JP22J01430 to H.N., JP21H04774, JP23H04766, JP24H00567 to M.M., and JP17H06332,

JP22H02762, JP23K18134, JP23H04696, JP25K02406, JP25H02543 to Y.N.), AMED-PRIME (JP22gm6110025 to Y.N.), JST FOREST Program (JPMJFR233E to Y.N.), The Mochida Memorial Foundation for Medical and Pharmaceutical Research (Y.N.), The Cell Science Research Foundation (Y.N.), and Sadako O. Hirai Ban Award for Young Researchers (H.N.)

Author contributions

Conceptualization: Y.A., Y.N.
Investigation: Y.A., H.N., Y.N.
Methodology: Y.A., H.N., T. F., A.T., Y.N.
Validation: Y.A., H.N., M.M., T. F., A.T., Y.N.
Data curation: Y.A., Y.N.
Writing – original draft: Y.A., H.N., Y.N.
Writing – review & editing: Y.A., H.N., A.T., M.M., Y.N.
Supervision: M.M., Y.N.
Funding acquisition: H.N., M.M., Y.N.

Declaration of interests

The authors declare no competing interests.

Materials and methods

Drosophila stock and maintenance

All stocks were maintained on a standard diet containing 4% cornmeal, 6% baker's yeast (Saf Yeast), 6% glucose (Wako, 049-31177), and 0.8% agar (Kishida chemical, 260-01705) with 0.3% propionic acid (Tokyo Chemical Industry, P0500) and 0.05% nipagin (Wako, 132-02635).

Canton-S was utilized as the wild-type strain. Transgenic fly lines were obtained from the Bloomington Drosophila Stock Center (BDSC), NIG-Fly and the Kyoto Stock Center. Unless otherwise indicated, strain descriptions can be

540 found at Flybase (http://flybase.bio.indiana.edu): *Dl-lacZ* (Röttgen et al.,
541 1998) (BDSC 11651), *esg-QF2* (Nagai et al., 2023), *QUAS-Fly-FUCCI* (Zielke et
542 al., 2014) (BDSC 55108), *BubR1*^{k03113} (Kyoto 102258), *BubR1*^{k06109} (Kyoto
543 102444), *mad2*^{EY} (Bellen et al., 2011) (BDSC 22495), *tub-Gal80*^{ts} (BDSC 7017,
544 7019, described in Flybase and BDSC), *esg-Gal4* (Goto & Hayashi, 1999)
545 (Kyoto 109126), *UAS-GFP* (BDSC 1521), *UAS-Cas9.T2A.eGFP* (Trivedi et al.,
546 2020) (BDSC 94298), *FRT40A* (originated from BDSC 5074), *attP40{U6-gRNA}*
547 (NIG 2RG-1578). The following lines were gifts from fly community: *esg-*
548 *GFP[P01986]* (Le Bras & Van Doren, 2006), *Su(H)GBE-lacZ* (Furriols & Bray,
549 2001), *yw hs-flp; tub-Gal80 FRT40A; tub-Gal4 UAS-dsRed /TM6B* (Guo et al.,
550 2013), *EGFP::BubR1*^{WT} (Shinoda et al., 2023), *GFP-BubR1, GFP-Mad2* (Buffin
551 et al., 2005), *mad2*$^{\Delta}$ (Buffin et al., 2007), *CycB-GFP* (Huang & Raff, 1999). The
552 following other *Drosophila* species were obtained from KYORIN-Fly: *D.*
553 *bifasciata* (JZK3), *D. triauraria* (TM15-92), *D. triauraria* (KMJ1), *D. triauraria*
554 (OEB12). See Additional file: Table S1 for the genotypes in each figure. We
555 used female flies unless otherwise noted in the figures.
556
557 **Diapause and recovery induction**
558 To assess the effects of diapause on midgut growth using *D. melanogaster*, we
559 subjected old virgin females less than 6 h to 10°C and 8 L:16D photoperiods
560 (Diapause condition), and 18°C at 12L:12D photoperiods (Control condition) for
561 1-5 weeks. We then allowed the flies to recover by transferring them into vials
562 with fresh food with dry yeast for 7 days at 25°C and 12L:12D photoperiods
563 (Recovery condition).
564 To assess the effects of the cold on midgut size, we allowed the flies to
565 grow in 18°C for 4 days after eclosion, and then subjected them to 10°C and
566 8 L:16D photoperiods for 3 weeks (Cold condition).
567 To assess the effects of diapause state on midgut growth in other
568 *Drosophila* species, we subjected virgin females less than 6 h old to 10 L:14D
569 photoperiods (SD, diapause) and 16L:8D photoperiods (LD, control) for 16 days.
570 The rearing temperature was kept consistent at 15°C. We then allowed the flies
571 to recover by transferring them into 16L:8D photoperiod condition.
572

573 **MARCM clone induction scheme**

574 For the mosaic analysis with a repressible cell marker (MARCM) analysis,
575 MARCM-ready flies (*hsFLP; tub-Gal80,FRT40A/FRT40A; tub-Gal4,UAS-dsRed*)
576 were cultured at 25°C throughout pupal development, except during heat shock
577 induction. When female larvae began metamorphosis, white pupae were placed
578 into an empty vial at 25°C and designated as being at 0 h after puparium
579 formation (APF). MARCM labels one of the two daughter cells after mitotic
580 division. To label dividing ISCs, MARCM-ready flies were heat shocked at 48 h
581 APF for 1 h (the time during which ISCs undergo asymmetric divisions (Guo &
582 Ohlstein, 2015)). After eclosion, the size of the growing ISC clones was observed
583 with anti-Pros immunofluorescence staining under 1 week diapause or 1 week
584 control conditions. EE-only clones, which can be induced by labeling daughter
585 EE during asymmetric division were excluded by immunostaining against the EE
586 marker Pros, and the size of clones containing two or more ISCs was quantified.

587

588 **Tissue-specific somatic mutation of BubR1**

589 Transgenic flies expressing BubR1-sgRNA (GGTGACGCCAGTTACTATTG)
590 obtained from NIG gRNA stock collections were crossed to flies
591 expressing *esg^{ts}>Cas9* (*esg-Gal4 tubGal80^{ts} / CyO; UAS-Cas9 / TM3, Act-GFP*).
592 Experimental crosses were maintained at 18°C to utilize Gal80^{ts} for suppressing
593 Gal4 activity. When female larvae began metamorphosis, white pupae were
594 placed into an empty vial at 18°C. After 6 days, when ISC division was completed,
595 pupae were transferred to 29°C and reared for 1 day to introduce somatic
596 mutations. These pupae were then transferred back to 18°C and reared under
597 diapause or control conditions for 3 weeks after eclosion.

598

599 **Immunofluorescence**

600 Adult midgut samples were dissected in 1 × PBS and fixed in 4% PFA for 30–
601 45 min at room temperature (RT). The following primary antibodies were used
602 with indicated dilution into 1 × PBS containing 0.5% BSA and 0.1% Triton X-100:
603 rabbit anti-PH3 (Millipore 06–570, 1:1000), mouse anti-Prospero (DSHB MR1A,
604 1:100), rat anti-GFP (Nacalai tesque 04404–26, 1:400), rabbit anti-cDcp1 (Cell
605 Signaling Technology 9578, 1:200), chicken anti-β-galactosidase (Abcam ab9361,

606 1:500), and mouse anti-Delta (DSHB C594.9B, 1:100). After overnight incubation
607 with primary antibodies at 4°C, samples were incubated with fluorescent
608 secondary antibodies (Jackson ImmunoResearch and Invitrogen, 1:500) for 1 h
609 at RT. Hoechst 33,342 (Invitrogen, final concentration: 10 μg/ml) was used to
610 visualize DNA. Samples were mounted in Slowfade Diamond (ThermoFisher,
611 S36963) and imaged with a Zeiss LSM880 confocal microscope.
612
613 **RT-qPCR**
614 Total RNA was purified from 7-10 midguts using the ReliaPrep RNA Tissue
615 Miniprep System (Promega). cDNA was made from 100 or 200 ng of RNA using
616 PrimeScript RT Reagent Kit (TaKaRa). Quantitative PCR was performed using
617 TB Green Premix Ex Taq II (TaKaRa) and the QuantStudio 6 Flex Real-Time PCR
618 System (ThermoFisher). *RpL32* was used as an internal control. Primers for *D.*
619 *bifasciata* and *D. triauraria* were designed based on the sequence homology to
620 *D. melanogaster* transcripts. Primer sequences are listed in Table S2.
621
622 **Bulk RNA-seq**
623 Total RNA was purified from 10 to 15 midguts using the ReliaPrep RNA Tissue
624 Miniprep System (Promega). A NanoDrop (ThermoFisher) was used to measure
625 the concentration of each RNA sample, and the integrity of RNA samples was
626 checked using a Bioanalyzer (Agilent). A total of 300 ng RNA for each sample
627 was used for cDNA library preparation and the subsequent sequencing was
628 performed on an DNB sequencing system with single reads of 50 base pairs. The
629 sequencing reads were aligned against the *Drosophila melanogaster* genome
630 (ENSEMBL, BDGP6.22) using Salmon (Patro et al., 2017) for transcript
631 quantification. The quantification data of each transcript was converted into gene-
632 level counts using Tximport (Soneson et al., 2015). Differential expression
633 analysis of two conditions/group (four biological replicates per condition) was
634 performed using the DESeq2 R package (ver 3.20). Genes with an adjusted *P*-
635 value < 0.1 were assigned as differentially expressed. For functional cluster
636 analysis of DEGs, GO BP enrichment analysis and Reactome pathway analysis
637 were performed with the ClusterProfiler R package.
638

639 **Colchicine treatment**

640 0.2 mM Colchicine was dissolved in 5% (w/v) sucrose solution. Filter paper
641 (Whatman 3MM) was soaked with 300 μL of reagents and placed into empty vials.
642 Newly-eclosed flies were transferred into these vials and fed with 5% sucrose
643 only (control) or colchicine solutions for 1 day.

644

645 **Starvation resistance**

646 To assay the starvation resistance, flies were fed with agar only food. For the
647 survival assay, dead flies (determined by immobility and a lack of response to
648 tapping) were counted daily.

649

650 **Quantification of midgut size**

651 The central line length and area of the midgut were quantified using the
652 Fiji/ImageJ free hand tool on images obtained with a Zeiss AXIO Zoom.V16
653 stereomicroscope.

654

655 **Quantification of cell number**

656 Cell number was quantified using Fiji/ImageJ. To count the total cell and *esg-*
657 *GFP*$^{+}$ cell number, Hoechst and GFP signal was processed as follows: (1)
658 despeckle, (2) binarization, (3) watershed, (4) analyze particle. Cell counts for
659 PH3^{+} cells, *Su(H)GBE-lacZ*$^{+}$ cells, and Fly-Fucci^{+} cells were manually counted
660 using the cell counter function.

661 For MARCM clone size quantification, clones containing two or more
662 ISCs were selected, and the number of cells in the clone was counted manually.

663

664 **Quantification of signal intensity**

665 The signal intensity of reporter lines (*EGFP::BubR1*^{WT}*, GFP-Mad2*) was
666 quantified using Fiji/ImageJ. The signal areas were selected as ROIs using the
667 polygon selection tool. The reporter intensity in each ROI was quantified using
668 the Measure command.

669

670 **Statistics**

671 Statistical analyses were performed using Excel and RStudio. Two-tailed *t* tests

were used for comparisons between two groups. One-way ANOVAs with post hoc Tukey tests were performed when comparing three or more groups. Log-rank tests were used for survival curve comparison. Significance is indicated in the figures as follows: $*P \leq 0.05$, $**P \leq 0.01$, $***P \leq 0.001$, not significant (N.S.): $P > 0.05$. Bar graphs show mean ± standard error. Boxplots show median (thick line in the box), first and third quartiles (bottom and top of the box), minimum value (lower whisker), and maximum value (upper whisker). Dots in bar graphs and boxplots indicate individual values. Violin plots portray the distribution of individual values.

Figure legends

Figure 1. The adult midgut of *Drosophila* undergoes remodeling in response to diapause and recovery

(A) Schematic of diapause and recovery in *D. melanogaster*. LD = Light : Dark.

(B) Representative images of the midgut under the 3 weeks diapause (3wD) and recovery (3wD+R) condition. The two orange lines indicate anterior and posterior end of the midgut. Scale bars: 1 mm.

(C, D) Quantification of midgut length of wild-type flies (Canton-S) under diapause and control conditions (C) and their recovery conditions (D). *n*=10-15 midguts for each condition. The same diapause samples are quantified in (C) and (D).

(E) Quantification of midgut length and area in the anterior and posterior region. Canton-S was analyzed. *n*=6 (3wC), 9 (3wD), and 21 (3wD+R) midguts for length measurements and *n*=15 (3wC), 20 (3wD), 17(3wD+R) midguts for area measurements.

(F) Quantification of midgut length and area in the anterior and posterior region. w^{1118} was analyzed. *n*=10 (3wC), 10 (3wD), 15 (3wD+R) midguts for length measurements and *n*=10 (3wC), 11 (3wD), 15 (3wD+R) midguts for area measurements.

(G) Female adult of *D. bifasciata* (JZK3) and *D. triauraria* (TM15-92). Scale bars: 1 mm.

(H) Schematic of diapause and recovery conditions in *D. bifasciata* and *D.*

705 *triauraria.* Light: Dark= 16 : 8 (hours) for long day (LD) condition, 10 : 14 (hours)
706 for short day (SD) condition.
707 (I) Representative images of the midgut in *D. bifasciata* (JZK3) under control (LD),
708 diapause (SD), and recovery conditions. Scale bars: 1 mm.
709 (J, K) Quantification of midgut length in *D. bifasciata* (J) and *D. triauraria* (K). *n*=7-
710 12 midguts for each condition.
711
712 **Figure 2. ISCs maintain cell cycle arrest and mitotic inhibition throughout**
713 **diapause**
714 (A, B) Schematics of the structure (A) and cell types (B) of the adult midgut of
715 *D. melanogaster*. An intestinal stem cell (ISC) generates an enteroblast (EB) or
716 an enteroendocrine progenitor (EEP), which differentiates into an enterocyte
717 (EC) or an enteroendocrine cell (EE), respectively.
718 (C) Total cell number in the adult midgut of wild-type flies under 3 weeks control
719 (3wC), 3 weeks diapause (3wD), and recovery after 3 weeks diapause (3wD+R).
720 *n*=7 (3wC), 8 (3wD), 8 (3wD+R) midguts.
721 (D) Representative images of *esg-GFP*$^{+}$ cells in the posterior midgut under 3wC
722 and 3wD conditions. Scale bars: 100 μm.
723 (E) Quantification of *esg-GFP*$^{+}$ cell number. *n*=11 (3wC), 12 (3wD), 10 (3wD+R)
724 midguts.
725 (F) Representative images of anti-PH3 staining in 3wC and 3wD wild-type flies.
726 Scale bars: 100 μm.
727 (G) PH3+ cell number in the anterior and posterior regions of 3wC and 3wD flies.
728 *n*=6 (3wC), 8 (3wD) midguts.
729 (H) Schematics of MARCM clone induction. ISC was labeled before eclosion, and
730 clonal expansion was examined at 1 week after eclosion.
731 (I) Representative images of MARCM clones in 1wC and 1wD conditions. A single
732 clone derived from an ISC is enclosed within the orange lines. Scale bars: 50 μm.
733 (J) Quantification of clone size. *n*=21 (1wC),10 (1wD) clones.
734 (K, L) Representative images of the Fly-Fucci signals in the progenitor (esg+)
735 cells (K). Scale bars: 100 μm. The proportion of G2/M (GFP+ and RFP+ cells) is
736 higher under the 3wD condition (L). *n*=7 (3wC), 5 (3wD) midguts.
737

Figure 3. BubR1 expression increases in the cytoplasm of ISCs during diapause

(A) MA plot of differentially expressed genes in a pair-wise comparison of 3wC and 3wD conditions.

(B, C) Gene ontology (GO) enrichment for upregulated genes (B) and downregulated genes (C) in 3wD.

(D) Cell-cycle-related GO terms (biological process, BP) enriched in 3wD (left) and heat map of “cell cycle checkpoint signaling" genes (right). These GO terms were identified through enrichment analysis of all differentially expressed genes.

(E) Expression level of *BubR1* in 3wC and 3wD midguts from RNA-seq data. Count data was normalized with RLE (Relative Log Expression). *n*=4 (3wC), 4 (3wD) RNA samples.

(F) Representative images of EGFP::BubR1 in the midgut under 3wC and 3wD conditions. Scale bars: 50 μm.

(G) Quantification of the EGFP::BubR1 signal intensity of (F). 30 cells from 4 midguts (3wC), 41 cells from 4 midguts (3wD).

(H) Representative images of BubR1 localization in ISCs. BubR1 is localized in the cytosol under the 3wD condition while BubR1 is accumulated at the kinetochore (KT) after colchicine treatment. Scale bars: 10 μm.

(I) The proportion of BubR1 localization in mitotic (PH3+) cells. 215 cells from 6 midguts (3wD), 31 cells from 4 midguts (Colchicine fed fly).

Figure 4. BubR1 expression in ISCs is essential for DDMR

(A) RT-qPCR of *BubR1* in control and *BubR1* heterozygous mutant flies under the 3wC and 3wD condition. *n*=4 (3wC, w^{1118}), 3 (3wC, $BubR1^{k06109}$/+), 4 (3wC, $BubR1^{k03113}$/+), 4 (3wD, w^{1118}), 4 (3wD, $BubR1^{k06109}$/+), 4 (3wD, $BubR1^{k03113}$/+) RNA samples.

(B) Representative images of the midgut in control and *BubR1* heterozygous mutant flies under the 3wD conditions. Scale bars: 1 mm.

(C) Quantification of the midgut length in control, *BubR1* heterozygous mutant, and $EGFP::BubR1^{WT}$ flies under 3wD. In $EGFP::BubR1^{WT}$ flies, wild-type form of *BubR1* is BAC rescued in the *BubR1* trans-heterozygous mutant background. *n*=27 (w^{1118}), 22 ($BubR1^{k06109}$/+), 18 ($BubR1^{k03113}$/+), 23 ($EGFP::BubR1^{WT}$)

771 midguts.
772 (D) Total cell number in control, *BubR1* heterozygous mutants, and
773 *EGFP::BubR1*^{WT} rescue flies under 3wD. *n*=10 (*w*^{1118}), 10 (*BubR1*^{k06109}/+), 15
774 (*BubR1*^{k03113}/+), 23 (*EGFP::BubR1*^{WT}) midguts.
775 (E) PH3+ cell number in control, *BubR1* heterozygous mutants, and
776 *EGFP::BubR1*^{WT} rescue flies under 3wD. *n*=16 (*w*^{1118}), 10 (*BubR1*^{k06109}/+), 15
777 (*BubR1*^{k03113}/+), 22 (*EGFP::BubR1*^{WT}) midguts.
778 (F) Quantification of *esg*+ cell number in control, *BubR1* heterozygous mutants
779 under 3wD. *n*=23 (*w*^{1118}), 11 (*BubR1*^{k06109}/+), 16 (*BubR1*^{k03113}/+) midguts.
780 (G) Schematic of CRISPR-mediated *BubR1* knockout in *esg*+ cells.
781 (H) Quantification of midgut length in control and *esg*+-specific *BubR1* knockout
782 flies. *n*=10 (*esg*^{Cas9}>+),10 (*esg*^{Cas9}>*BubR1*^{CRISPR}) midguts.
783 (I) Total cell number in control and *esg*+-specific *BubR1* knockout flies. *n*=9
784 (*esg*^{Cas9}>+),9 (*esg*^{Cas9}>*BubR1*^{CRISPR}) midguts.
785 (J) PH3+ cell number in control and *esg*+-specific *BubR1* knockout flies. *n*=10
786 (*esg*^{Cas9}>+),10 (*esg*^{Cas9}>*BubR1*^{CRISPR}) midguts.
787
788 **Figure 5. The MCC component Mad2 is involved in DDMR**
789 (A) Expression level of *mad2* in 3wC and 3wD midguts from RNA-seq data. Count
790 data was normalized with RLE.
791 (B) Representative images of *GFP-Mad2* midguts under 3wC and 3wD conditions.
792 (C) Quantification of GFP-Mad2 signal intensity of (B). 40 cells from 4 midguts
793 (3wC), 52 cells from 4 midguts (3wD).
794 (D) Representative images of the midgut in control and *mad2* heterozygous
795 mutant flies under 3wD. Scale bars: 1 mm.
796 (E) Quantification of midgut length in control and *mad2* heterozygous mutant flies
797 under 3wD. *n*=12 (*w*^{1118}), 9 (*mad2*$^{\Delta}$/+), 7 (*mad2*^{EY}/+) midguts. The same *w*^{1118}
798 control samples were used in Figure 5E and Figure 4C.
799 (F) Quantification of *esg*+ cell number in control and *mad2* heterozygous mutant
800 flies under 3wD. *n*=23 (*w*^{1118}), 10 (*mad2*$^{\Delta}$/+), 6 (*mad2*^{EY}/+) midguts. The *w*^{1118}
801 control are same sample as in Figure 4E.
802 (G) Starvation resistance in control and *BubR1* heterozygous mutant flies. *n*=128
803 (*w*^{1118}), 114 (*BubR1*^{k06109}/+), 103 (*BubR1*^{k03113}/+) flies.

(H) Graphical summary of midgut remodeling in diapause and recovery conditions.

Figure S1. Midgut remodeling in coordination with *Drosophila* reproductive diapause

(A) Representative image of ovary growth arrest in *D. melanogaster* diapause. Scale bar: 1 mm.

(B) Schematic of control and recovery in *D. melanogaster*. LD = Light : Dark.

(C) Quantification of midgut length of wild-type flies (Canton-S) under control and recovery conditions. *n*=6-13 midguts for each condition. The control samples are same as in Figure 1C.

(D) Quantification of midgut length in the recovery condition for 1-7 days. *n*=8-21 midguts for each condition.

(E) Schematic of the diapause and cold conditions in *D. melanogaster*. LD = Light : Dark. To set up the cold condition, we allowed the flies to grow in 18°C for 4 days after eclosion, and then held them at 10 °C with 8 L:16D photoperiods for 3 weeks.

(F) Quantification of midgut length under diapause and cold conditions after 3 weeks. *n*=9-21 midguts for each condition. The 3 weeks diapause samples are the same shown in Figure 1C.

(G) Quantification of midgut length and area in wild-type male flies (Canton-S) under 3wC and 3wD condition. *n*=7 (3wC), 7 (3wD) midguts.

(H) Representative images of ovaries in *D. bifasciata* (JZK3) and *D. triauraria* (TM15-92) under long day (LD) and short day (SD) conditions. In SD, ovarian growth arrest was induced. Scale bars: 1 mm.

(I, J) Quantification of midgut length of non-diapause strains of *D. triauraria* (KMJ1 and OEB12) under LD and SD conditions. *n*=11 (KMJ1, LD), 11 (KMJ1, SD), 8 (OEB12, LD), 13 (OEB12, SD) midguts. KMJ1 and OEB12 female flies do not enter diapause state in the SD condition (Yamada & Yamamoto, 2011).

Figure S2. ISCs remain in a non-proliferative state during diapause

(A) The proportion of esg+ cells in total cells. *n*=11 (3wC), 12 (3wD), 10 (3wD+R) midguts.

837 (B) Representative images of the posterior midgut under 3wC and 3wD
838 conditions in *Dl-lacZ* flies. Scale bars: 100 μm.
839 (C) Representative images of anti-Dl staining in 3wC and 3wD wild-type flies.
840 Scale bars: 100 μm.
841 (D) Representative images of the posterior midgut under 3wC and 3wD
842 conditions in *Su(H)GBE-lacZ* flies. Scale bars: 100 μm.
843 (E) Quantification of the Su(H)+ cell number. *n*=8 (3wC), 6 (3wD) midguts.
844 (F) The proportion of Su(H)+ cells in total cells. *n*=8 (3wC), 6 (3wD) midguts.
845 (G) PH3+ cell number in the midgut of 3wC, 3wD, and 3wD+R flies. n=6 (3wC),
846 8 (3wD), 6 (3wD+R) midguts. The 3wC and 3wD samples are the same shown in
847 Figure 2F.
848 (H) Representative images of the posterior midgut under 3wC and 3wD
849 conditions in *CycB-GFP* flies. Scale bars: 100 μm.
850 (I) Representative images of anti-cDcp1 staining in 3wC and 3wD wild-type flies.
851 Scale bars: 50 μm.
852
853 **Figure S3. Molecular signatures identified by RNA-seq analysis in DDMR**
854 (A) Gene ontology (GO) enrichment of 3wD transcriptome compared to 3wC. All
855 differentially expressed genes in 3wD are used for enrichment analysis.
856 (B) Reactome Pathway Enrichment in 3wD compared to 3wC. All differentially
857 expressed genes in 3wD are used for enrichment analysis.
858 (C) Expression levels of *bmm, pepck, tobi* from RNA-seq data. *n*=4 (3wC), 4
859 (3wD) RNA samples. Count data was normalized with RLE.
860 (D) Expression levels of *per, tim* from RNA-seq data. *n*=4 (3wC), 4 (3wD) RNA
861 samples. Count data was normalized with RLE.
862 (E) Expression levels of *Drs* from RNA-seq data. *n*=4 (3wC), 4 (3wD) RNA
863 samples. Count data was normalized with RLE.
864 (F) Representative images of GFP-BubR1 from 3wC and 3wD posterior midguts.
865 Scale bar: 100 μm.
866 (G) MA plot of differentially expressed genes in a pair-wise comparison of 3wC+R
867 and 3wD+R conditions.
868 (H) GO enrichment in 3wD+R compared to 3wC+R. All differentially expressed
869 genes in 3wD+R are used for enrichment analysis.

(I) Reactome Pathway Enrichment in 3wD+R compared to 3wC+R. All differentially expressed genes in 3wD+R are used for enrichment analysis.
(J) Expression levels of *CCHa2, Dh31, dilp3, NPF, Thor* from RNA-seq data. *n*=4 (3wC+R), 4 (3wD+R) RNA samples. Count data was normalized with RLE.

Figure S4. BubR1 functions in the midgut in coordination with *Drosophila* reproductive diapause

(A) Quantification of midgut length in control and *BubR1* heterozygous mutants under 3wC. *n*=10 (w^{1118}), 8 ($BubR1^{k06109}$/+), 8 ($BubR1^{k03113}$/+) midguts.
(B) PH3+ cell number in control, *BubR1* heterozygous mutants, and *EGFP::BubR1*^{WT} flies under 3wC. *n*=10 (w^{1118}), 8 ($BubR1^{k06109}$/+), 8 ($BubR1^{k03113}$/+) midguts.
(C) RT-qPCR of *BubR1* in control and CRISPR-mediated *BubR1* knockout flies under the 3wD condition. *n*=9 (esg^{Cas9}>+), 9 (esg^{Cas9}>$BubR1^{CRISPR}$) RNA samples.
(D) RT-qPCR of *BubR1* in *D. bifasciata* (JZK3) midgut under the control (LD) and diapause (SD) conditions. *n*=8 (LD), 9 (SD) RNA samples.
(E) RT-qPCR of *BubR1* in *D. triauraria* (TM15-92) midgut under the control (LD) and diapause (SD) conditions. *n*=6 (LD), 8 (SD) RNA samples.

References

Anduaga, A. M., Nagy, D., Costa, R., & Kyriacou, C. P. (2018). Diapause in Drosophila melanogaster – Photoperiodicity, cold tolerance and metabolites. *Journal of Insect Physiology*, *105*, 46–53. https://doi.org/10.1016/j.jinsphys.2018.01.003

Baker, D. J., Dawlaty, M. M., Wijshake, T., Jeganathan, K. B., Malureanu, L., Van Ree, J. H., Crespo-Diaz, R., Reyes, S., Seaburg, L., Shapiro, V., Behfar, A., Terzic, A., Van De Sluis, B., & Van Deursen, J. M. (2013). Increased expression of BubR1 protects against aneuploidy and cancer and extends healthy lifespan. *Nature Cell Biology*, *15*(1), 96–102. https://doi.org/10.1038/ncb2643

Baker, D. J., Jeganathan, K. B., Cameron, J. D., Thompson, M., Juneja, S., Kopecka, A., Kumar, R., Jenkins, R. B., De Groen, P. C., Roche, P., & Van Deursen, J. M. (2004). BubR1 insufficiency causes early onset of aging-associated phenotypes and infertility in mice. *Nature Genetics*, *36*(7), 744–749. https://doi.org/10.1038/ng1382

Bellen, H. J., Levis, R. W., He, Y., Carlson, J. W., Evans-Holm, M., Bae, E., Kim, J., Metaxakis, A., Savakis, C., Schulze, K. L., Hoskins, R. A., & Spradling, A. C. (2011). The Drosophila gene disruption project: Progress using transposons with distinctive site specificities. *Genetics*, *188*(3), 731–743. https://doi.org/10.1534/genetics.111.126995

Bier, E., Harrison, M. M., O'connor-Giles, K. M., & Wildonger, J. (2018). Advances in engineering the fly genome with the CRISPR-Cas system. *Genetics*, *208*(1), 1–18. https://doi.org/10.1534/genetics.117.1113

Buchon, N., Osman, D., David, F. P. A., Yu Fang, H., Boquete, J. P., Deplancke, B., & Lemaitre, B. (2013). Morphological and Molecular Characterization of Adult Midgut Compartmentalization in Drosophila. *Cell Reports*, *3*(5), 1725–1738. https://doi.org/10.1016/j.celrep.2013.04.001

Buffin, E., Emre, D., & Karess, R. E. (2007). Flies without a spindle checkpoint. *Nature Cell Biology*, *9*(5), 565–572. https://doi.org/10.1038/ncb1570

Buffin, E., Lefebvre, C., Huang, J., Gagou, M. E., & Karess, R. E. (2005). Recruitment of Mad2 to the Kinetochore Requires the Rod/Zw10 Complex. *Current Biology*, *15*(9), 856–861. https://doi.org/10.1016/j.cub.2005.03.052

Choi, E., Zhang, X., Xing, C., & Yu, H. (2016). Mitotic Checkpoint Regulators Control Insulin Signaling and Metabolic Homeostasis. *Cell*, *166*(3), 567–581. https://doi.org/10.1016/j.cell.2016.05.074

Christensen, C. F., Laurichesse, Q., Loudhaief, R., Colombani, J., & Andersen, D. S. (2024). Drosophila activins adapt gut size to food intake and promote regenerative growth. *Nature Communications*, *15*(1), 273. https://doi.org/10.1038/s41467-023-44553-9

Denlinger, D. L. (2022). *Insect Diapause* (Vol. 464). Cambridge University Press. https://doi.org/10.1017/9781108609364

DiVito Evans, A., Fairbanks, R. A., Schmidt, P., & Levine, M. T. (2023). Histone methylation regulates reproductive diapause in Drosophila melanogaster.

PLOS Genetics, *19*(9), e1010906. https://doi.org/10.1371/journal.pgen.1010906

Easwaran, S., & Montell, D. J. (2023). The molecular mechanisms of diapause and diapause-like reversible arrest. In *Biochemical Society Transactions* (Vol. 51, Issue 5, pp. 1847–1856). Portland Press Ltd. https://doi.org/10.1042/BST20221431

Easwaran, S., & Montell, D. J. (2024). *A genome-wide association study implicates the olfactory system in Drosophila melanogaster diapause-associated lifespan extension and fecundity*. https://doi.org/10.7554/eLife.98142.2

Easwaran, S., Van Ligten, M., Kui, M., & Montell, D. J. (2022). Enhanced germline stem cell longevity in Drosophila diapause. *Nature Communications*, *13*(1). https://doi.org/10.1038/s41467-022-28347-z

Fang, Y., Liu, T., Wang, X., Yang, Y. M., Deng, H., Kunicki, J., Traganos, F., Darzynkiewicz, Z., Lu, L., & Dai, W. (2006). BubR1 is involved in regulation of DNA damage responses. *Oncogene*, *25*(25), 3598–3605. https://doi.org/10.1038/sj.onc.1209392

Goto, S., & Hayashi, S. (1999). Proximal to distal cell communication in the *Drosophila* leg provides a basis for an intercalary mechanism of limb patterning. *Development*, *126*(15), 3407–3413. https://doi.org/10.1242/dev.126.15.3407

Gray, D. R., Logan, J. A., Ravlin, F. W., & Carlson, J. A. (1991). Toward a Model of Gypsy Moth Egg Phenology: Using Respiration Rates of Individual Eggs to Determine Temperature–Time Requirements of Prediapause Development. *Environmental Entomology*, *20*(6), 1645–1652. https://doi.org/10.1093/ee/20.6.1645

Guo, Z., Driver, I., & Ohlstein, B. (2013). Injury-induced BMP signaling negatively regulates *Drosophila* midgut homeostasis. *Journal of Cell Biology*, *201*(6), 945–961. https://doi.org/10.1083/jcb.201302049

Guo, Z., & Ohlstein, B. (2015). Bidirectional Notch signaling regulates Drosophila intestinal stem cell multipotency. *Science*, *350*(6263), 927. https://doi.org/10.1126/science.aab0988

Hara, Y., & Yamamoto, D. (2022). Effects of Food and Temperature on Drosophila

melanogaster Reproductive Dormancy as Revealed by Quantification of a GFP-Tagged Yolk Protein in the Ovary. *Frontiers in Physiology*, *12*. https://doi.org/10.3389/fphys.2021.803144

Harsimran Kaur Gill, Gaurav Goyal, & Gurminder Chahil. (2017). Insect Diapause: A Review. *Journal of Agricultural Science and Technology A*, *7*(7). https://doi.org/10.17265/2161-6256/2017.07.002

Helfrich-Förster, C. (2024). Neuropeptidergic regulation of insect diapause by the circadian clock. In *Current Opinion in Insect Science* (Vol. 63). Elsevier Inc. https://doi.org/10.1016/j.cois.2024.101198

Huang, J.-Y., & Raff, J. W. (1999). The disappearance of cyclin B at the end of mitosis is regulated spatially in Drosophila cells. In *The EMBO Journal* (Vol. 18, Issue 8). https://www.embopress.org

Hung, R.-J., Hu, Y., Kirchner, R., Liu, Y., Xu, C., Comjean, A., Tattikota, S. G., Li, F., Song, W., Ho Sui, S., & Perrimon, N. (2020). A cell atlas of the adult *Drosophila* midgut. *Proceedings of the National Academy of Sciences*, *117*(3), 1514–1523. https://doi.org/10.1073/pnas.1916820117

Karess, R. E., Wassmann, K., & Rahmani, Z. (2013). New insights into the role of BubR1 in mitosis and beyond. In *International Review of Cell and Molecular Biology* (Vol. 306, pp. 223–273). Elsevier Inc. https://doi.org/10.1016/B978-0-12-407694-5.00006-7

Karp, X. (2021). Hormonal Regulation of Diapause and Development in Nematodes, Insects, and Fishes. In *Frontiers in Ecology and Evolution* (Vol. 9). Frontiers Media S.A. https://doi.org/10.3389/fevo.2021.735924

Kim, M., & Denlinger, D. L. (2009). Decrease in expression of beta-tubulin and microtubule abundance in flight muscles during diapause in adults of Culex pipiens. *Insect Molecular Biology*, *18*(3), 295–302. https://doi.org/10.1111/j.1365-2583.2009.00870.x

Kim, M., Robich, R. M., Rinehart, J. P., & Denlinger, D. L. (2006). Upregulation of two actin genes and redistribution of actin during diapause and cold stress in the northern house mosquito, Culex pipiens. *Journal of Insect Physiology*, *52*(11–12), 1226–1233. https://doi.org/10.1016/j.jinsphys.2006.09.007

Kimura, M. T. (1990). Quantitative response to photoperiod during reproductive diapause in the Drosophila auraria species-complex. *Journal of Insect*

Physiology, *36*(3), 147–152. https://doi.org/10.1016/0022-1910(90)90115-V

Kubrak, O. I., Kučerová, L., Theopold, U., & Nässel, D. R. (2014). The sleeping beauty: How reproductive diapause affects hormone signaling, metabolism, immune response and somatic maintenance in Drosophila melanogaster. *PLoS ONE*, *9*(11). https://doi.org/10.1371/journal.pone.0113051

Kubrak, O. I., Kucerová, L., Theopold, U., Nylin, S., & Nässel, D. R. (2016). Characterization of reproductive dormancy in male Drosophila melanogaster. *Frontiers in Physiology*, *7*(NOV). https://doi.org/10.3389/fphys.2016.00572

Kučerová, L., Kubrak, O. I., Bengtsson, J. M., Strnad, H., Nylin, S., Theopold, U., & Nässel, D. R. (2016). Slowed aging during reproductive dormancy is reflected in genome-wide transcriptome changes in Drosophila melanogaster. *BMC Genomics*, *17*(1). https://doi.org/10.1186/s12864-016-2383-1

Kurogi, Y., Imura, E., Mizuno, Y., Hoshino, R., Nouzova, M., Matsuyama, S., Mizoguchi, A., Kondo, S., Tanimoto, H., Noriega, F. G., & Niwa, R. (2023). Female reproductive dormancy in Drosophila is regulated by DH31-producing neurons projecting into the corpus allatum. *Development (Cambridge, England)*, *150*(10). https://doi.org/10.1242/dev.201186

Kurtz, C. C., Otis, J. P., Regan, M. D., & Carey, H. V. (2021). How the gut and liver hibernate. In *Comparative Biochemistry and Physiology -Part A : Molecular and Integrative Physiology* (Vol. 253). Elsevier Inc. https://doi.org/10.1016/j.cbpa.2020.110875

LAKOVAARA, S., SAURA, A., KOREF-SANTIBAÑEZ, S., & EHRMAN, L. E. E. (1972). Aspects of diapause and its genetics in northern drosophilids. *Hereditas*, *70*(1), 89–96. https://doi.org/https://doi.org/10.1111/j.1601-5223.1972.tb00996.x

Le Bras, S., & Van Doren, M. (2006). Development of the male germline stem cell niche in Drosophila. *Developmental Biology*, *294*(1), 92–103. https://doi.org/10.1016/j.ydbio.2006.02.030

Li, H., & Jasper, H. (2016). Gastrointestinal stem cells in health and disease: from flies to humans. *Disease Models & Mechanisms*, *9*(5), 487–499. https://doi.org/10.1242/dmm.024232

Lirakis, M., Dolezal, M., & Schlötterer, C. (2018). Redefining reproductive

dormancy in Drosophila as a general stress response to cold temperatures. *Journal of Insect Physiology*, *107*, 175–185. https://doi.org/10.1016/j.jinsphys.2018.04.006

Liu, M., Yang, S., Yang, J., Feng, P., Luo, F., Zhang, Q., Yang, L., & Jiang, H. (2024). BubR1 controls starvation-induced lipolysis via IMD signaling pathway in Drosophila. *Aging*, *16*(4), 3257–3279. https://doi.org/10.18632/aging.205533

Malita, A., Kubrak, O., Koyama, T., Ahrentløv, N., Texada, M. J., Nagy, S., Halberg, K. V., & Rewitz, K. (2022). A gut-derived hormone suppresses sugar appetite and regulates food choice in Drosophila. *Nature Metabolism*, *4*(11), 1532–1550. https://doi.org/10.1038/s42255-022-00672-z

Marianes, A., & Spradling, A. C. (2013). Physiological and stem cell compartmentalization within the Drosophila midgut. *ELife*, *2*. https://doi.org/10.7554/eLife.00886

Mattila, J., Viitanen, A., Fabris, G., Strutynska, T., Korzelius, J., & Hietakangas, V. (2024). Stem cell mTOR signaling directs region-specific cell fate decisions during intestinal nutrient adaptation. *Science Advances*, *10*(6). https://doi.org/10.1126/sciadv.adi2671

McGuire, S. E., Le, P. T., Osborn, A. J., Matsumoto, K., & Davis, R. L. (2003). Spatiotemporal Rescue of Memory Dysfunction in *Drosophila*. *Science*, *302*(5651), 1765–1768. https://doi.org/10.1126/science.1089035

Meiselman, M. R., Alpert, M. H., Cui, X., Shea, J., Gregg, I., Gallio, M., & Yapici, N. (2022). Recovery from cold-induced reproductive dormancy is regulated by temperature-dependent AstC signaling. *Current Biology*, *32*(6), 1362-1375.e8. https://doi.org/10.1016/j.cub.2022.01.061

Meller, C. L., Meller, R., Simon, R. P., Culpepper, K. M., Podrabsky, J. E., Meller, C., Lynn, ;, Meller, R. ;, Simon, R. P. ;, & Culpepper, K. M. ; (2012). Cell Cycle Arrest Associated with Anoxia-Induced Quiescence, Anoxic Preconditioning, and Embryonic Diapause in Embryos of the Annual Killifish Austrofundulus Limnaeus Citation Details. In *Biology Faculty Publications and Presentations Biology*. https://pdxscholar.library.pdx.edu/bio_fac/47

Meltzer, H., Marom, E., Alyagor, I., Mayseless, O., Berkun, V., Segal-Gilboa, N., Unger, T., Luginbuhl, D., & Schuldiner, O. (2019). Tissue-specific (ts)CRISPR

as an efficient strategy for in vivo screening in Drosophila. *Nature Communications*, *10*(1), 2113. https://doi.org/10.1038/s41467-019-10140-0

Meyerhof, G. T., Easwaran, S., Bontempo, A. E., Montell, C., & Montell, D. J. (2024). Altered circadian rhythm, sleep, and *rhodopsin 7* –dependent shade preference during diapause in *Drosophila melanogaster*. *Proceedings of the National Academy of Sciences*, *121*(27). https://doi.org/10.1073/pnas.2400964121

Miguel-Aliaga, I., Jasper, H., & Lemaitre, B. (2018). Anatomy and Physiology of the Digestive Tract of *Drosophila melanogaster*. *Genetics*, *210*(2), 357–396. https://doi.org/10.1534/genetics.118.300224

Musacchio, A. (2015). The Molecular Biology of Spindle Assembly Checkpoint Signaling Dynamics. In *Current Biology* (Vol. 25, Issue 20, pp. R1002–R1018). Cell Press. https://doi.org/10.1016/j.cub.2015.08.051

Nagai, H., Miura, M., & Nakajima, Y. ichiro. (2022). Cellular mechanisms underlying adult tissue plasticity in Drosophila. In *Fly* (Vol. 16, Issue 1, pp. 190–206). Taylor and Francis Ltd. https://doi.org/10.1080/19336934.2022.2066952

Nagai, H., Nagai, L. A. E., Tasaki, S., Nakato, R., Umetsu, D., Kuranaga, E., Miura, M., & Nakajima, Y. (2023). Nutrient-driven dedifferentiation of enteroendocrine cells promotes adaptive intestinal growth in Drosophila. *Developmental Cell*, *58*(18), 1764-1781.e10. https://doi.org/10.1016/j.devcel.2023.08.022

Nakagaki, M., Takei, R., Nagashima, E., & Yaginuma, T. (1991). Cell cycles in embryos of the silkworm, Bombyx mori: G2-arrest at diapause .stage. In *Arch Dev Biol* (Vol. 200).

O'Brien, L. E., Soliman, S. S., Li, X., & Bilder, D. (2011). Altered modes of stem cell division drive adaptive intestinal growth. *Cell*, *147*(3), 603–614. https://doi.org/10.1016/j.cell.2011.08.048

Ojima, N., Hara, Y., Ito, H., & Yamamoto, D. (2018). Genetic dissection of stress-induced reproductive arrest in Drosophila melanogaster females. *PLoS Genetics*, *14*(6). https://doi.org/10.1371/journal.pgen.1007434

Park, J., Hall, C., Hubbard, B., LaMoia, T., Gaspar, R., Nasiri, A., Li, F., Zhang, H., Kim, J., Haeusler, R. A., Accili, D., Shulman, G. I., Yu, H., & Choi, E.

(2023). MAD2-Dependent Insulin Receptor Endocytosis Regulates Metabolic Homeostasis. *Diabetes*, *72*(12), 1781–1794. https://doi.org/10.2337/db23-0314

Patro, R., Duggal, G., Love, M. I., Irizarry, R. A., & Kingsford, C. (2017). Salmon provides fast and bias-aware quantification of transcript expression. *Nature Methods*, *14*(4), 417–419. https://doi.org/10.1038/nmeth.4197

Reiff, T., Jacobson, J., Cognigni, P., Antonello, Z., Ballesta, E., Tan, K. J., Yew, J. Y., Dominguez, M., & Miguel-Aliaga, I. (2015). Endocrine remodelling of the adult intestine sustains reproduction in Drosophila. *ELife*, *4*. https://doi.org/10.7554/eLife.06930

Resende, L. P., Monteiro, A., Brás, R., Lopes, T., & Sunkel, C. E. (2018). Aneuploidy in intestinal stem cells promotes gut dysplasia in Drosophila. *Journal of Cell Biology*, *217*(11), 3930–3946. https://doi.org/10.1083/jcb.201804205

Röttgen, G., Wagner, T., & Hinz, U. (1998). A genetic screen for elements of the network that regulates neurogenesis in Drosophila. *Molecular and General Genetics MGG*, *257*(4), 442–451. https://doi.org/10.1007/s004380050668

Saunders, D. S., Henricht, V. C., & Gilbertt, L. I. (1989). Induction of diapause in Drosophila melanogaster: Photoperiodic regulation and the impact of arrhythmic clock mutations on time measurement (ovarian diapause). In *Genetics* (Vol. 86).

Saunders, D. S., Richard, D. S., Applebaum, S. W., Ma, M., & Gilbert~, L. I. (1990). Photoperiodic Diapause in Drosophila melanogaster Involves a Block to the Juvenile Hormone Regulation of Ovarian Maturation. In *GENERAL AND COMPARATIVE ENDOCRINOLOGY* (Vol. 79).

Schiesari, L., Andreatta, G., Kyriacou, C. P., O'Connor, M. B., & Costa, R. (2016). The insulin-like proteins dILPs-2/5 determine diapause inducibility in Drosophila. *PLoS ONE*, *11*(9). https://doi.org/10.1371/journal.pone.0163680

Schiesari, L., & O'Connor, M. B. (2013). *Diapause* (pp. 213–246). https://doi.org/10.1016/B978-0-12-396968-2.00008-7

Shinoda, N., Horikoshi, M., Taira, Y., Muramoto, M., Hirayama, S., Murata, S., & Miura, M. (2023). Caspase cleaves Drosophila BubR1 to modulate spindle assembly checkpoint function and lifespan of the organism. *FEBS Journal*,

290(17), 4200–4223. https://doi.org/10.1111/febs.16811

Soneson, C., Love, M. I., & Robinson, M. D. (2015). Differential analyses for RNA-seq: transcript-level estimates improve gene-level inferences. *F1000Research*, *4*, 1521. https://doi.org/10.12688/f1000research.7563.2

Song, Y.-H. (2005). Drosophila melanogaster: a model for the study of DNA damage checkpoint response. *Molecules and Cells*, *19*(2), 167–179.

Staples, J. F. (2016). Metabolic Flexibility: Hibernation, Torpor, and Estivation. In *Comprehensive Physiology* (pp. 737–771). Wiley. https://doi.org/10.1002/cphy.c140064

Stojanović, O., Miguel-Aliaga, I., & Trajkovski, M. (2022). Intestinal plasticity and metabolism as regulators of organismal energy homeostasis. *Nature Metabolism*, *4*(11), 1444–1458. https://doi.org/10.1038/s42255-022-00679-6

Tammariello, S. P., & Denlinger, D. L. (1998). G0/G1 Cell Cycle Arrest in the Brain of Sarcophaga crassipalpis During Pupal Diapause and the Expression Pattern of the Cell Cycle Regulator, Proliferating Cell Nuclear Antigen. In *Insect Biochem. Molec. Biol* (Vol. 28, Issue 2).

Tang, R., Jiang, Z., Chen, F., Yu, W., Fan, K., Tan, J., Zhang, Z., Liu, X., Li, P., & Yuan, K. (2020). The Kinase Activity of Drosophila BubR1 Is Required for Insulin Signaling-Dependent Stem Cell Maintenance. *Cell Reports*, *31*(12), 107794. https://doi.org/10.1016/j.celrep.2020.107794

Tatar, M., & Yin, C.-M. (2001). Slow aging during insect reproductive diapause: why butterflies, grasshoppers and flies are like worms. *Experimental Gerontology*, *36*(4–6), 723–738. https://doi.org/10.1016/S0531-5565(00)00238-2

Trivedi, D., Vinitha, C. M., Bisht, K., Janardan, V., Pandit, A., Basak, B., Shwetha, H., Ramesh, N., & Raghu, P. (2020). A genome engineering resource to uncover principles of cellular organization and tissue architecture by lipid signaling. *ELife*, *9*, 1–23. https://doi.org/10.7554/ELIFE.55793

Watabe, H. (1979). *Drosophila Survey of Hokkaido, XXXVI. Seasonal Changes in the Reproductive Condition of Wild and Domestic Species of Drosophila*.

White, M. A., Bonfini, A., Wolfner, M. F., & Buchon, N. (2021). *Drosophila melanogaster* sex peptide regulates mated female midgut morphology and physiology. *Proceedings of the National Academy of Sciences*, *118*(1).

https://doi.org/10.1073/pnas.2018112118

Wilsterman, K., Ballinger, M. A., & Williams, C. M. (2021). A unifying, eco-physiological framework for animal dormancy. *Functional Ecology*, *35*(1), 11–31. https://doi.org/10.1111/1365-2435.13718

Yamada, H., & Yamamoto, M. T. (2011). Association between circadian clock genes and diapause incidence in Drosophila triauraria. *PLoS ONE*, *6*(12). https://doi.org/10.1371/journal.pone.0027493

Yoshinari, Y., Nishimura, T., Yoshii, T., Kondo, S., Tanimoto, H., Kobayashi, T., Matsuyama, M., & Niwa, R. (2024). A high-protein diet-responsive gut hormone regulates behavioral and metabolic optimization in Drosophila melanogaster. *Nature Communications*, *15*(1), 10819. https://doi.org/10.1038/s41467-024-55050-y

Zhou, X., Ding, G., Li, J., Xiang, X., Rushworth, E., & Song, W. (2020). Physiological and Pathological Regulation of Peripheral Metabolism by Gut-Peptide Hormones in Drosophila. In *Frontiers in Physiology* (Vol. 11). Frontiers Media S.A. https://doi.org/10.3389/fphys.2020.577717

Zielke, N., Korzelius, J., vanStraaten, M., Bender, K., Schuhknecht, G. F. P., Dutta, D., Xiang, J., & Edgar, B. A. (2014). Fly-FUCCI: A Versatile Tool for Studying Cell Proliferation in Complex Tissues. *Cell Reports*, *7*(2), 588–598. https://doi.org/10.1016/j.celrep.2014.03.020

Figure 1

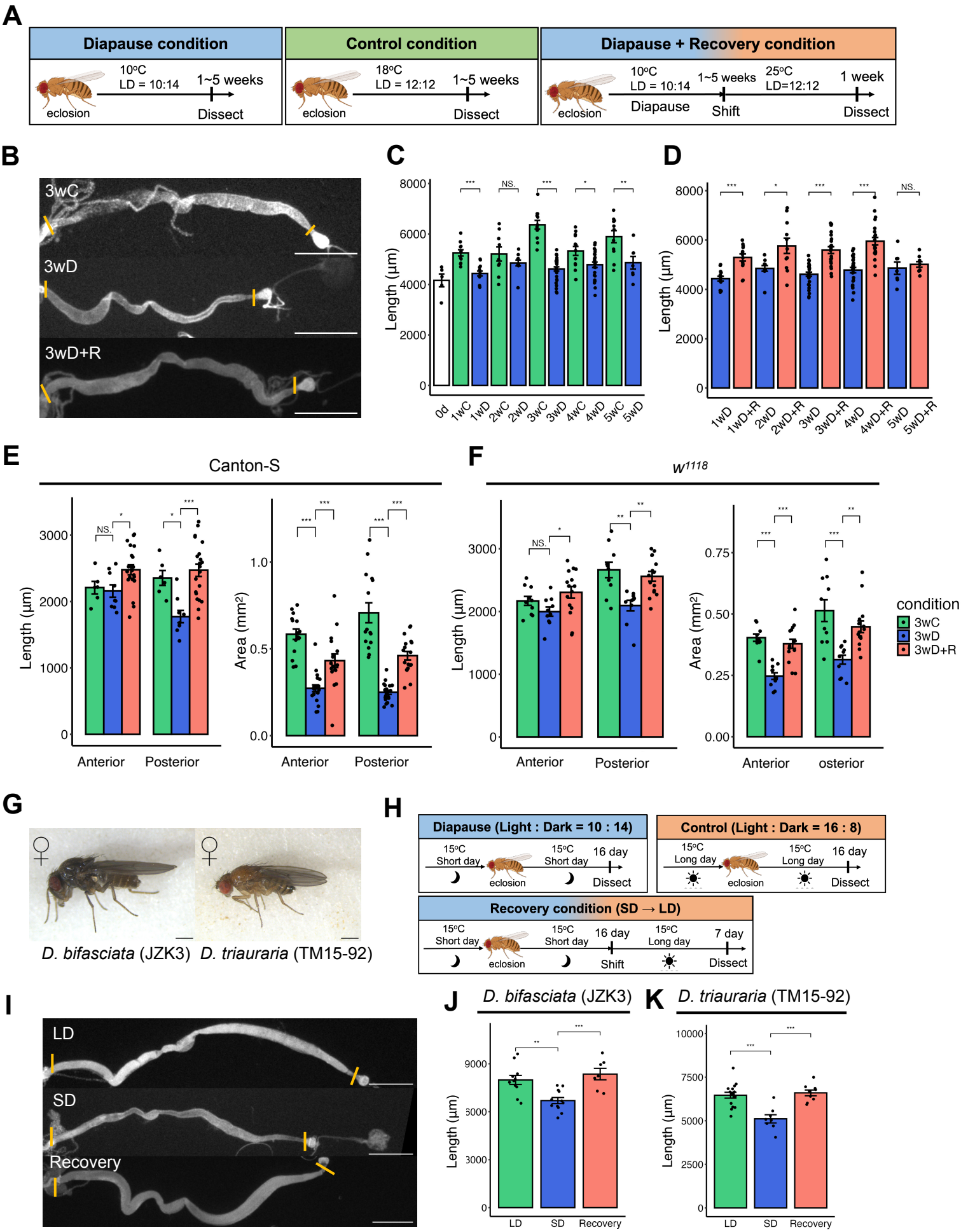
A
Diapause condition
10ºC
LD = 10:14
1~5 weeks
eclosion
Dissect
Control condition
18ºC
LD = 12:12
1~5 weeks
eclosion
Dissect
Diapause + Recovery condition
10ºC
LD = 10:14
1~5 weeks
25ºC
LD=12:12
1 week
eclosion
Diapause
Shift
Dissect
B
3wC
3wD
3wD+R
C
Length (µm)
0d
1wC
1wD
2wC
2wD
3wC
3wD
4wC
4wD
5wC
5wD
D
Length (µm)
1wD
1wD+R
2wD
2wD+R
3wD
3wD+R
4wD
4wD+R
5wD
5wD+R
E
Canton-S
Length (µm)
Area (mm²)
Anterior
Posterior
F
w1118
Length (µm)
Area (mm²)
Anterior
Posterior
osterior
condition
3wC
3wD
3wD+R
G
D. bifasciata (JZK3)
D. triauraria (TM15-92)
H
Diapause (Light : Dark = 10 : 14)
15ºC
Short day
eclosion
15ºC
Short day
16 day
Dissect
Control (Light : Dark = 16 : 8)
15ºC
Long day
eclosion
15ºC
Long day
16 day
Dissect
Recovery condition (SD → LD)
15ºC
Short day
eclosion
15ºC
Short day
16 day
Shift
15ºC
Long day
7 day
Dissect
I
LD
SD
Recovery
J
D. bifasciata (JZK3)
Length (µm)
LD
SD
Recovery
K
D. triauraria (TM15-92)
Length (µm)
LD
SD
Recovery

Figure 2

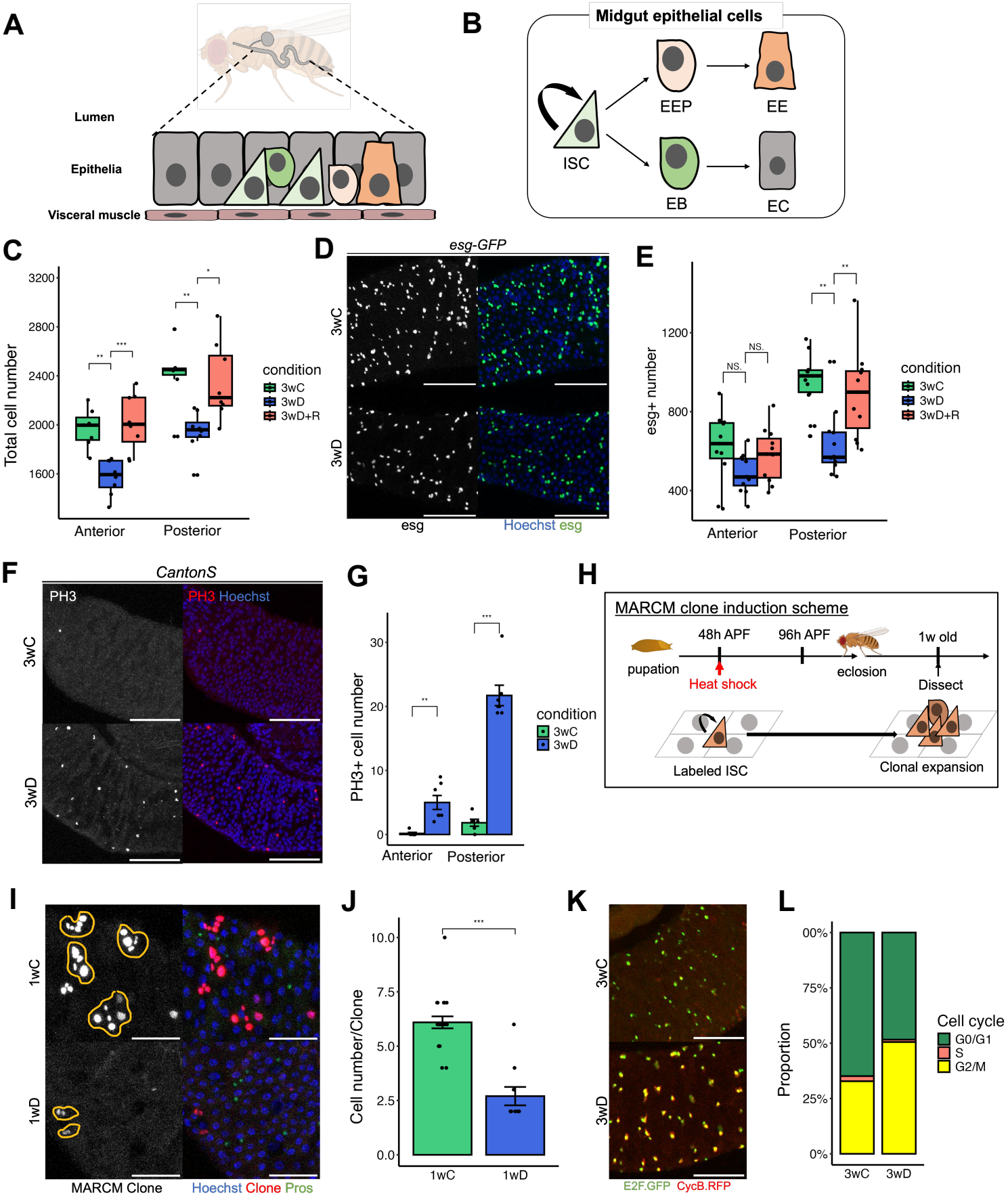
A
Lumen
Epithelia
Visceral muscle
B
Midgut epithelial cells
ISC
EEP
EE
EB
EC
C
Total cell number
condition
3wC
3wD
3wD+R
Anterior
Posterior
D
esg-GFP
3wC
3wD
esg
Hoechst esg
E
esg+ number
NS.
condition
3wC
3wD
3wD+R
Anterior
Posterior
F
CantonS
PH3
PH3 Hoechst
3wC
3wD
G
PH3+ cell number
condition
3wC
3wD
Anterior
Posterior
H
MARCM clone induction scheme
48h APF
96h APF
1w old
pupation
Heat shock
eclosion
Dissect
Labeled ISC
Clonal expansion
I
1wC
1wD
MARCM Clone
Hoechst Clone Pros
J
Cell number/Clone
1wC
1wD
K
3wC
3wD
E2F.GFP CycB.RFP
L
Proportion
Cell cycle
G0/G1
S
G2/M
3wC
3wD

Figure 3

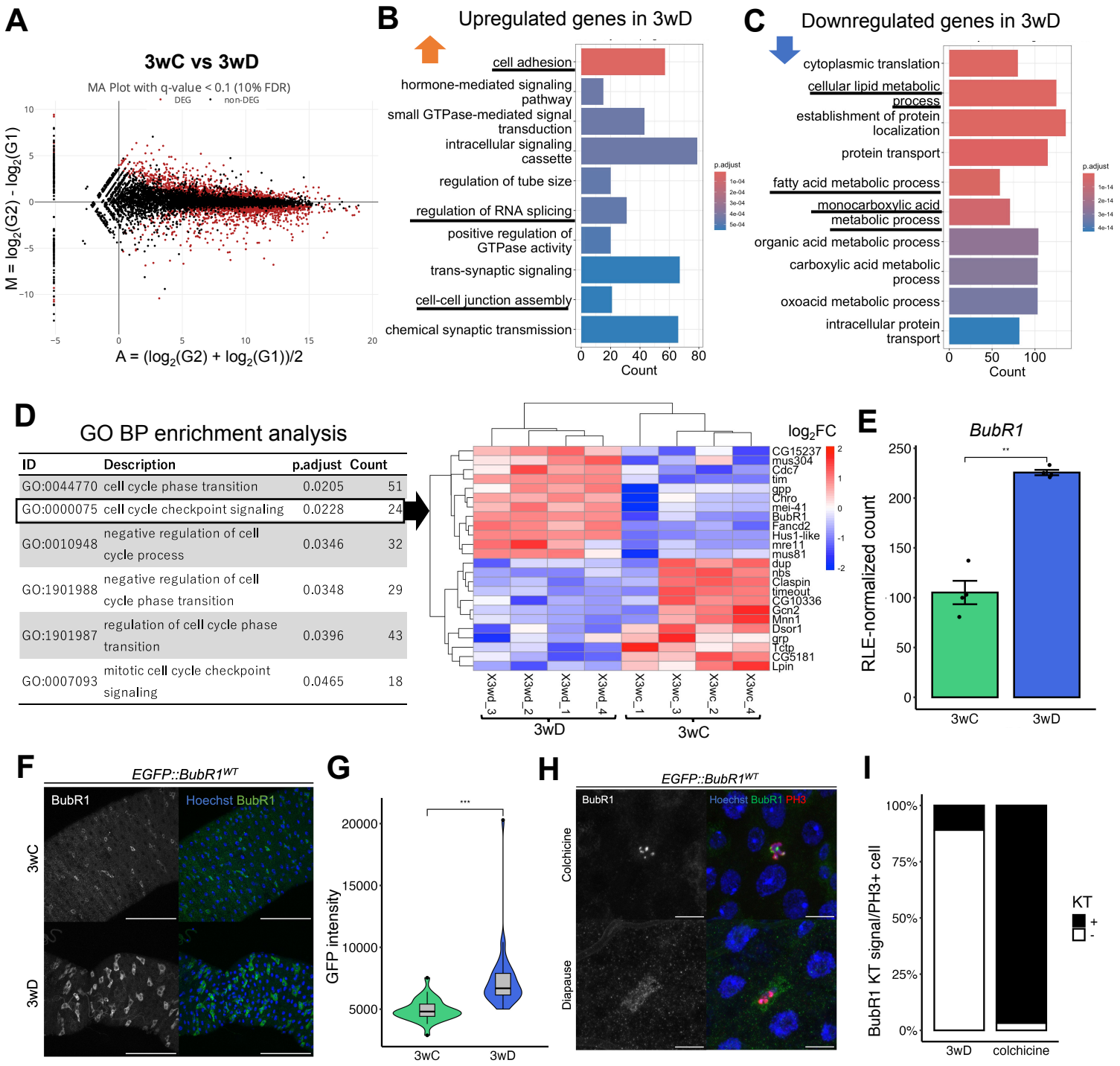
A
3wC vs 3wD
MA Plot with q-value < 0.1 (10% FDR)
DEG
non-DEG
M = log2(G2) - log2(G1)
A = (log2(G2) + log2(G1))/2
B
Upregulated genes in 3wD
cell adhesion
hormone-mediated signaling pathway
small GTPase-mediated signal transduction
intracellular signaling cassette
regulation of tube size
regulation of RNA splicing
positive regulation of GTPase activity
trans-synaptic signaling
cell-cell junction assembly
chemical synaptic transmission
Count
p.adjust
C
Downregulated genes in 3wD
cytoplasmic translation
cellular lipid metabolic process
establishment of protein localization
protein transport
fatty acid metabolic process
monocarboxylic acid metabolic process
organic acid metabolic process
carboxylic acid metabolic process
oxoacid metabolic process
intracellular protein transport
Count
p.adjust
D
GO BP enrichment analysis
ID Description p.adjust Count
GO:0044770 cell cycle phase transition 0.0205 51
GO:0000075 cell cycle checkpoint signaling 0.0228 24
GO:0010948 negative regulation of cell cycle process 0.0346 32
GO:1901988 negative regulation of cell cycle phase transition 0.0348 29
GO:1901987 regulation of cell cycle phase transition 0.0396 43
GO:0007093 mitotic cell cycle checkpoint signaling 0.0465 18
log2FC
CG15237
mus304
Cdc7
tim
gpp
Chro
mei-41
BubR1
Fancd2
Hus1-like
mre11
mus81
dup
nbs
Claspin
timeout
CG10336
Gcn2
Mnn1
Dsor1
grp
Tctp
CG5181
Lpin
X3wd_3
X3wd_2
X3wd_1
X3wd_4
X3wc_1
X3wc_3
X3wc_2
X3wc_4
3wD
3wC
E
BubR1
RLE-normalized count
3wC
3wD
F
EGFP::BubR1WT
BubR1
Hoechst BubR1
3wC
3wD
G
GFP intensity
3wC
3wD
H
EGFP::BubR1WT
BubR1
Hoechst BubR1 PH3
Colchicine
Diapause
I
BubR1 KT signal/PH3+ cell
KT
+
-
3wD
colchicine

Figure 4

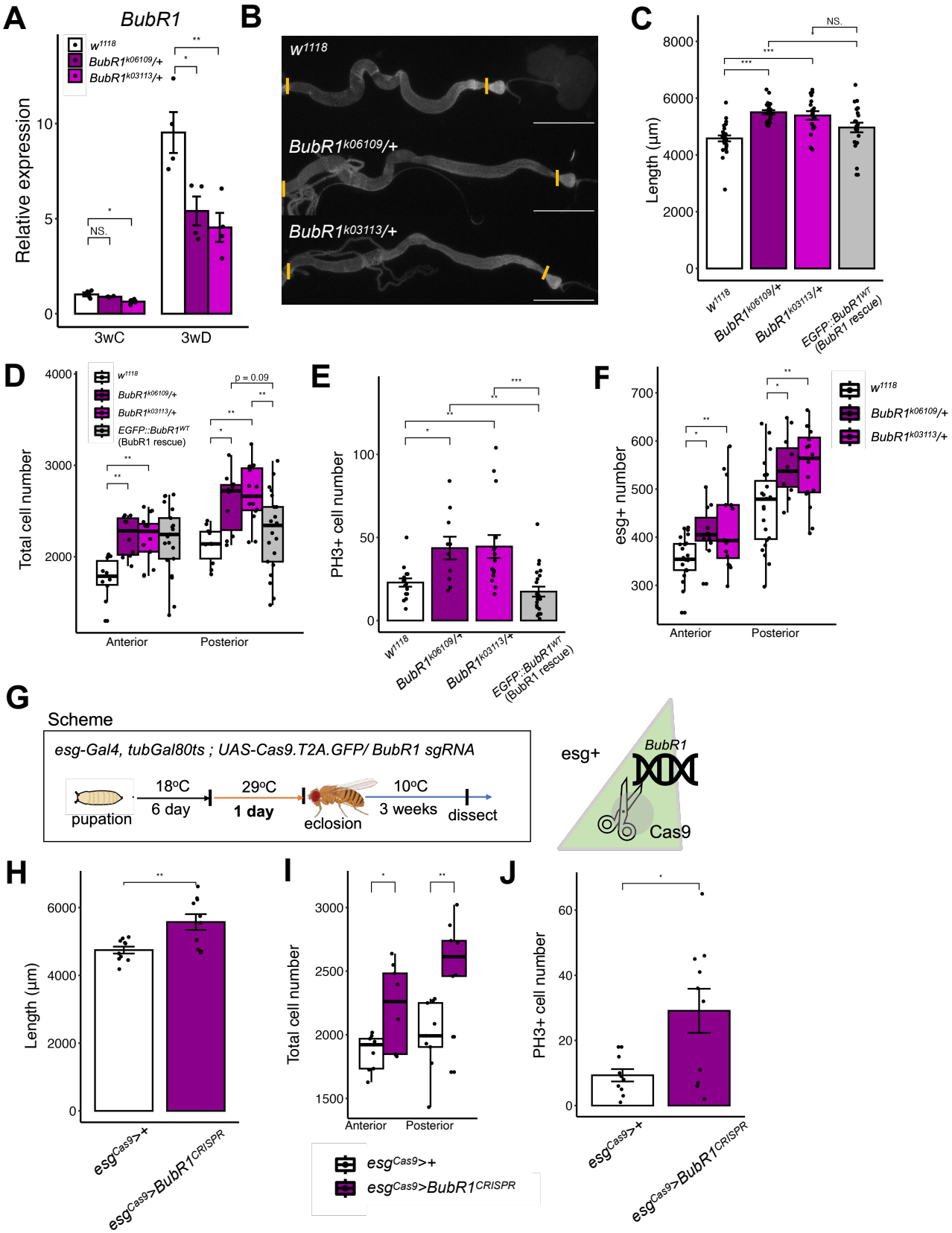
A
BubR1
w1118
BubR1k06109/+
BubR1k03113/+
Relative expression
NS.
3wC
3wD
B
w1118
BubR1k06109/+
BubR1k03113/+
C
Length (µm)
NS.
w1118
BubR1k06109/+
BubR1k03113/+
EGFP::BubR1WT (BubR1 rescue)
D
Total cell number
p = 0.09
EGFP::BubR1WT (BubR1 rescue)
Anterior
Posterior
E
PH3+ cell number
F
esg+ number
Anterior
Posterior
G
Scheme
esg-Gal4, tubGal80ts ; UAS-Cas9.T2A.GFP/ BubR1 sgRNA
pupation
18ºC
6 day
29ºC
1 day
eclosion
10ºC
3 weeks
dissect
esg+
BubR1
Cas9
H
Length (µm)
esgCas9>+
esgCas9>BubR1CRISPR
I
Total cell number
Anterior
Posterior
esgCas9>+
esgCas9>BubR1CRISPR
J
PH3+ cell number
esgCas9>+
esgCas9>BubR1CRISPR

Figure 5

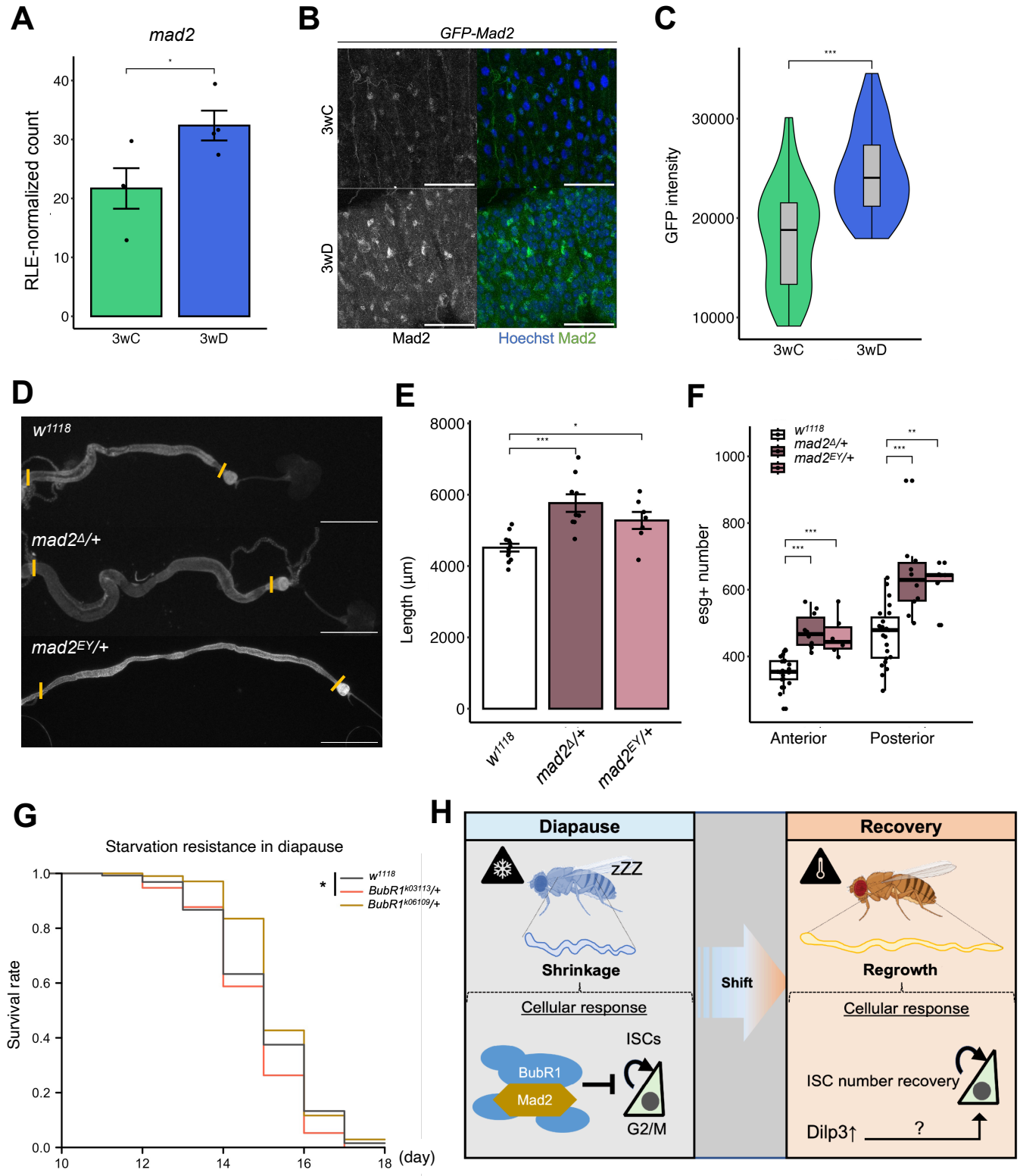
A
mad2
RLE-normalized count
3wC
3wD
B
GFP-Mad2
3wC
3wD
Mad2
Hoechst Mad2
C
GFP intensity
3wC
3wD
D
w1118
mad2Δ/+
mad2EY/+
E
Length (μm)
w1118
mad2Δ/+
mad2EY/+
F
esg+ number
w1118
mad2Δ/+
mad2EY/+
Anterior
Posterior
G
Starvation resistance in diapause
Survival rate
(day)
w1118
BubR1k03113/+
BubR1k06109/+
H
Diapause
Recovery
zZZ
Shrinkage
Shift
Regrowth
Cellular response
Cellular response
ISCs
BubR1
Mad2
G2/M
ISC number recovery
Dilp3↑
?